Memoirs of the Faculty of Science, Kyoto University, Series of Physics, Astrophysics, Geophysics and Chemistry, Vol. XXXVI, No. 1, Article 1, 1981

DIFFERENTIAL CROSS SECTIONS FOR THE REACTION $\gamma n \to \pi^\circ n$ AT PHOTON ENERGIES BETWEEN 300 MeV AND 700 MeV

By

Yosuke INAGAKI

Department of Physics, Faculty of Science, Kyoto University, Kyoto

(*Received February 1, 1979*)

ABSTRACT

The differential cross section for the reaction $\gamma n \to \pi^\circ n$ have been measured at four pi-zero c.m. angles of 70°, 90°, 110° and 130° in the photon energy region between 300 MeV and 700 MeV. Both π° mesons and recoil neutrons from a liquid deuterium target were detected with a pair of lead glass Cerenkov counters and a nucleon hodoscope. The extraction of the differential cross sections on free neutrons from the reaction $\gamma d \to \pi^\circ np_s$ is discussed in detail. Deuteron corrections to the cross sections are about 20% in the $\Delta(1232)$ resonance region. The differential cross sections for $\gamma n \to \pi^\circ n$ show good agreement with the predictions of MOR and MW in this energy region. There is no enhancement of the cross section due to the $N(1470)P_{11}$ resonance. No positive evidence for an isotensor electromagnetic current is found.

CONTENTS

I. Introduction

The investigation of single pion photoproduction in the resonance region has

provided useful information about nucleon resonant states. The couplings of the individual resonant states to the γN system has been determined by the extensive partial wave analyses of the experimental data. For the major resonances the experimental results were in good agreement with the quark model,[1-4] but the values for the small coupled resonances were not well determined by the analyses. For a systematic analysis of single pion photoproduction, more precise and more extensive differential cross section data, as well as polarization data of various kinds of $\gamma N \to \pi N$ reactions are needed. The experimental data for the $\gamma p \to \pi^+ n$, $\gamma p \to \pi^\circ p$ and $\gamma n \to \pi^- p$ reactions have been extensively accumulated[5-8], but the reaction $\gamma n \to \pi^\circ n$ has been scarcely investigated.[9-12] There is no cross section data on π° photoproduction from neutrons in the first resonance region because of difficulties on extraction of cross sections from the deuterium data. These deuteron problems have not yet completely understood for many reasons[13]: there is no direct proof of the validity of the spectator model, the final-state interactions and Glauber's rescattering terms cannot be calculated exactly.

In isospin space the electromagnetic current is written as a sum of isoscalar and isovector terms. In 1971, the possible existence of an electromagnetic isotensor current was suggested by Sanda and Shaw[14] who analyzed the cross sections for photo-excitation of the $\Delta(1232)$ on protons and neutrons. Furthermore the possibility of a violation of time reversal invariance was pointed out from a comparison of the two reactions $\gamma n \to \pi^- p$ and $\pi^- p \to \gamma n$ in the $\Delta(1232)$ region[15]. In order to clarify the above situation, counter experiments on π^- photoproduction on neutrons have been performed at Bonn[16] and INS.[17] These groups measured the π^-/π^+ yield ratios on a deuterium target, as a function of the pion angles. In the ratios most deuteron effects are expected to cancel due to the charge symmetry of the final states. The results indicate that there is no isotensor current in photo-excitation of the $\Delta(1232)$ at the level of a few percent. On the other hand the experiment on the reaction $\gamma n \to \pi^\circ n$ provides a better test of the existence of the isotensor current. Since neutral pion photoproduction is almost completely dominated by the $\Delta(1232)$ resonance in the first resonance region, the effect of the isotensor term is larger than in the charged pion production.

The aim of this experiment on the π° photoproduction from neutrons is mainly to clarify the isotensor contribution in the $\Delta(1232)$ resonance region, to test the validity of the spectator model and to obtain more accurate experimental information on the isoscalar current in the second resonance region where the $I=1/2$ resonances $N(1470)P_{11}$, $N(1520)D_{13}$ and $N(1535)S_{11}$ are dominant amplitudes. We have measured the differential cross sections for the reactions $\gamma n \to \pi^\circ n$ and $\gamma p \to \pi^\circ p$ from a deuterium target at the same time at the π° c.m. angles of 70°, 90°, 110° and 130° in the photon energy range 300 MeV to 700 MeV, by detecting both π° mesons and recoil nucleons in coincidence.

The results on the ratios of the differential cross sections for the reactions $\gamma d \to \pi^\circ n p_s$ and $\gamma d \to \pi^\circ p n_s$ were reported in the thesis by N. Yamashita.[18]

In this paper, we present the differential cross sections for the reaction $\gamma n \to \pi^\circ n$ extracted from the $\gamma d \to \pi^\circ n p_s$ data. The paper is divided into five sections. In sect. 2, the experimental procedure in which the measurements have been made are described. Sect. 3 is devoted to discussions of the off-line data reduction. In sect. 4 we shall examine deuteron problems; in particular, we evaluate corrections needed to account for the Fermi motion, for the effects of double scattering and the final-state

interaction and for the Glauber screening effect. Finally, in sect. 5 we discuss the results.

II. Experimental Procedure

II-1. Method

In this experiment the differential cross sections for the following reactions have been measured simultaneously:

$$\gamma + d \to \pi^\circ + n + p_s \tag{1}$$

$$\gamma + d \to \pi^\circ + p + n_s . \tag{2}$$

The spectator proton p_s and the spectator neutron n_s are expected to have momentum smaller than that of the recoil nucleon and less than 250 MeV/c in any case. In order to identify the reaction (1) or (2), we measure both momenta of the π° meson and the recoil nucleon because of the continuous spectrum of bremsstrahlung photons and the moving nucleon in a deuterium target.

The bremsstrahlung beam from the 1.3 GeV electron synchrotron at the Institute for Nuclear Study was incidented on a deuterium target. The general lay-out of the experimental apparatus is shown in Fig. 1. The basic detection system is similar to

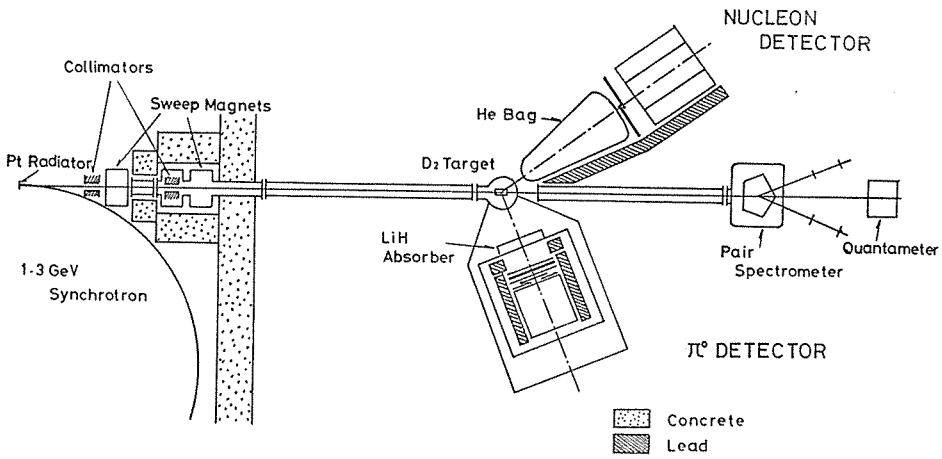

Fig. 1. Schematic lay-out of the experimental apparatus.

that of the previous experiment of Kyoto group.[9] The π° meson was detected by observing two decay photons with a pair of photon detectors having better resolutions and gains than those at previous experiment. Each photon detector consisted of a total absorption lead glass Čerenkov counter, a two dimensional scintillator hodoscope, a lead plate converter, a veto counter, a lead collimator and a LiH hardener as shown in Fig. 2. The energy of each decay photon from the π° meson was measured with a lead glass Cerenkov counter. The opening angle of the decay photons from the π° meson $\phi_{\gamma\gamma}$ was obtained from the shower position in the lead converter which were measured with the two dimensional scintillator hodoscope. The recoil nucleon was detected in a 4×4 array of plastic scintillation counters. To identify whether the

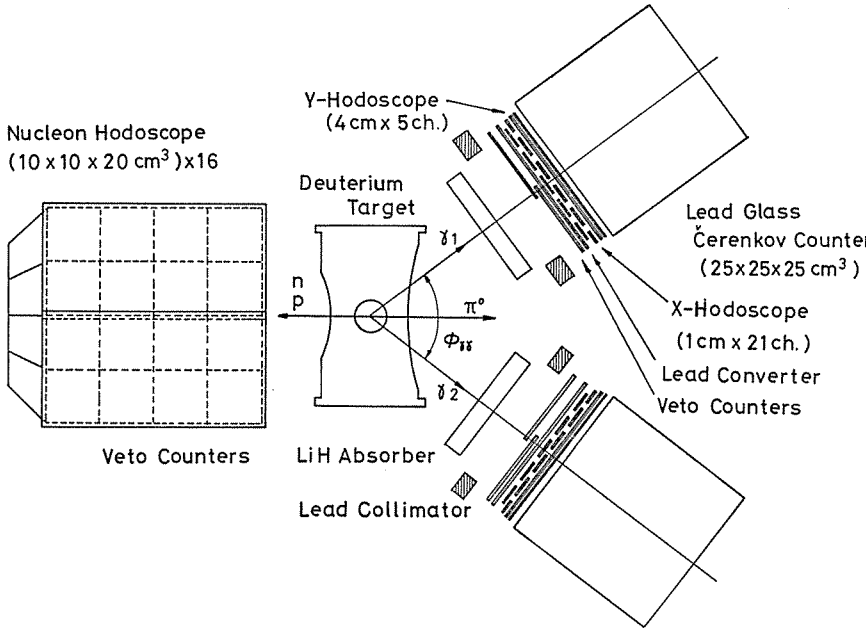

Fig. 2. Schematic front view of the π° detector and the nucleon detector.

recoil nucleon was a proton or a neutron, thin plastic scintillation counters were placed in front of the nucleon hodoscope. The kinetic energy of the recoil nucleon was measured with the time-of-flight method. These detectors were operated in coincidence and made it possible to measure the four momentum vectors of the π° meson and the recoil nucleon with high precision. The details of those counters are described in ref. 18.

II–2. Photon Beam

The photon beam was generated by bremsstrahlung from an internal radiator of 50 μm platinum in the INS 1.3 GeV electron synchrotron. The beam was defined by a lead collimator of 5 mm in diameter and 30 cm long placed at 2.5 m from the radiator. The second collimator of 12 mm in diameter was placed to reduce the beam haloes. Charged particles produced at the collimators were removed from the photon beam by the sweep magnets having a field strength of 7 KGauss. The diameter of the beam profile was 25 mm at the target position. The beam profile and its position were measured with polaroid films.

The fluctuation of the maximum energy of the bremsstrahlung beam was less than 0.2% by monitoring the field strength of synchrotron magnet and the energy indicator. The beam spill time was usually kept to be about 4 ms around the maximum field of the synchrotron magnet.

A thick-walled ionization chamber[19] was used as a beam intensity monitor. Collected charges from the thick chamber were sent to an integrator whose one digit we define as a monitor unit MU. Then the total energy U is obtained from the collected charge q in the thick chamber as follows:

$$U=\alpha q=\alpha\beta[MU], \tag{3}$$

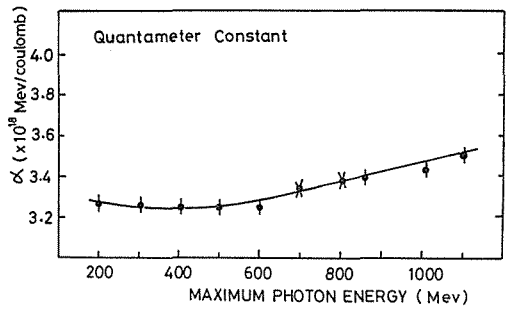

Fig. 3. Thick-walled ionization chamber constant curve.

where α and β denote the thick chamber constant (MeV/coulomb) and the integrator constant (coulomb/count), respectively. For example as shown in Fig. 3, α is 3.28×10^{18}MeV/coulomb at the maximum energy of 600 MeV. The thick chamber constant α was determined with an accuracy of 3% by calibration against a Faraday cup in the external electron beam. An equivalent quanta Q is defined by

$$Q = U/E_0 , \tag{4}$$

where E_0 is the maximum energy of the bremsstrahlung beam. The energy spectrum of the bremsstrahlung beam is given by the number of photons per energy interval dk

$$N(k)\mathrm{d}k = Q \frac{B(k)}{k} \mathrm{d}k. \tag{5}$$

The spectral function $B(k)$ was measured with a pair spectrometer. The function $B(k)$ at $E_0 = 750$ MeV is shown in Fig. 4 and found to agree with the Schiff's thin-target formula.

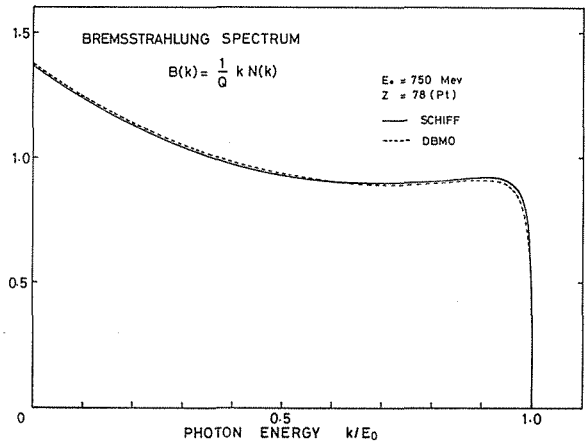

Fig. 4. Bremsstrahlung spectral function B(k) calculated by Schiff and Davies, Bethe, Maximon and Olsen.

II–3. Data Collection

The measurement of the reactions (1) and (2) using a liquid deuterium target has been performed at 13 points, these were 4 photon energies at 90°, 3 photon energies

at 70°, 110° and 130°. Details are given in ref. 18. The measurement of the reaction $\gamma p \to \pi^\circ p$ using a hydrogen target was also carried out in the same experimental arrangement at 90° runs.

III. Data Reduction

The differential cross sections for the reactions (1) and (2) were obtained from the following procedures:

1) event selections,
2) kinematical reconstruction,
3) corrections
4) Monte Carlo simulation,
5) reduction of the differential cross sections.

These procedures were performed in off-line analysis with computors TOSBAC-3400 at the INS and FACOM230/75 at the Computor Center of Kyoto University.

III-1. Event Selections

For each events the invariant mass of the two decay photons was calculated from the measured photon energies k'_1 and k'_2, and the opening angle of $\phi'_{\gamma\gamma}$. The events having the invariant mass close enough to the mass of π° mesons and having the appropriate time of flight of the recoil nucleans were selected as good events. The details of selection are also given in ref. 18.

III-2. Kinematical Reconstruction

The energy and momentum of a π° meson were precisely reconstructed from the measured energies and the opening angle of the two photons by using the following method.[20]

From energy-momentum conservation, the following eq. is derived:

$$k_1 \cdot k_2 = \frac{m^2_{\pi^\circ}}{2(1-\cos\phi_{\gamma\gamma})}, \tag{6}$$

where k_1, k_2 and $\phi_{\gamma\gamma}$ denote the energies of the decay photons from the π° meson and the opening angle between the two photons. In this experiment the accuracy of the measurement on the opening angle was better than that of the photon energies. The ambiguity of the left-hand term in eq. (6) was about 20 times as large as that of the right-hand term. Assuming that the ambiguity due to the opening angle is negligibly small, we define the right-hand term by A. The most probably photon energies (k_1, k_2) should be on the hyperbola $(k_1 \cdot k_2 = A)$ as shown in Fig. 5. Assuming that the measured energies (k'_1, k'_2) distribute around the true energies (k_1, k_2) on the hyperbola with a Gaussian type, the probability is given by

$$P(k_1, k_2) = \frac{1}{2\pi}\frac{1}{\sigma(k_1)\sigma(k_2)} \exp\left[-\frac{1}{2}\left\{\frac{(k_1-k'_1)^2}{\sigma^2(k_1)} + \frac{(k_2-k'_2)^2}{\sigma^2(k_2)}\right\}\right], \tag{7}$$

where $\sigma(k_i)$ denotes the deviation of the photon energy. Using the function defined by

$$f(k_1, k_2) = \frac{(k_1-k'_2)^2}{\sigma^2(k_1)} + \frac{(k_2-k'_2)^2}{\sigma^2(k_2)}, \tag{8}$$

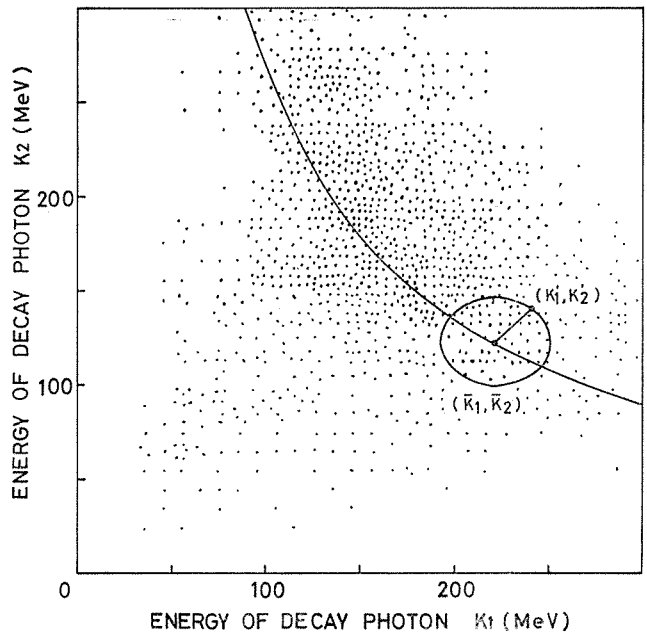

Fig. 5. Reconstruction of the energies of the two decay photons from the π° meson. (k_1', k_2') and $(\bar{k}_1, \bar{k}_2)$ denote the measured and the reconstructed photon energies for the 420–90°D run.

the most probable energies $\bar{k}_1$ and $\bar{k}_2$ are obained by minimizing the function $f(k_1, k_2)$. The energy resolution of a lead glass Čerenkov counter is approximated well by

$$\sigma(k_i) = c\sqrt{k_i} \quad (i=1, 2), \tag{9}$$

where c is a constant. From eq. (9) we can rewrite (8) by

$$\frac{(k_1-k_1')^2}{a^2} + \frac{(k_2-k_2')^2}{b^2} = 1, \tag{10}$$

where $a=\sqrt{k_1 \cdot f(k_1, k_2)}$ and $b=\sqrt{k_2 \cdot f(k_1, k_2)}$.
To minimize the function $f(k_1, k_2)$ is equivalent to minimize the area of the ellipse given by eq. (10). From eqs. (8) and (9), the most probable energies $\bar{k}_1$ and $\bar{k}_2$ can be easily obtained as follows:

$$\bar{k}_1 = \sqrt{\frac{k_1'^2+A}{k_1'^2+A}}\, A, \tag{11a}$$

$$\bar{k}_2 = \sqrt{\frac{k_2'^2+A}{k_1'^2+A}}\, A. \tag{11b}$$

The reconstructed energy and momentum of π° mesons were calculated for each event:

$$E_{\pi^\circ} = \bar{k}_1 + \bar{k}_2, \tag{12a}$$

$$\vec{p}_{\pi^\circ} = \vec{\bar{k}}_1 + \vec{\bar{k}}_2. \tag{12b}$$

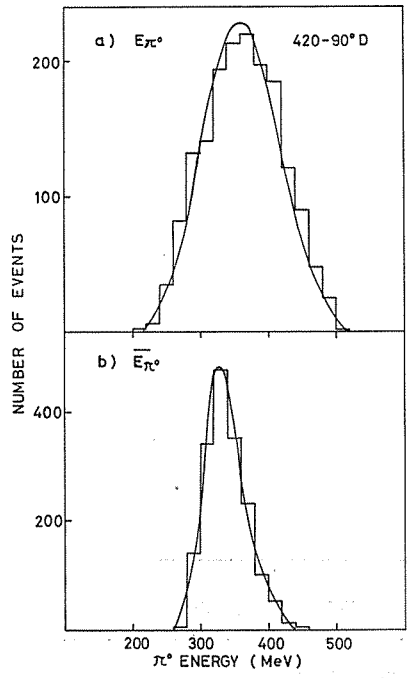

Fig. 6. a) π° energy calculated from the non-reconstructed energies of the two decay photons ($E'_{\pi^\circ}=k'_1+k'_2$) and b) the reconstructed energies ($E_{\pi^\circ}=\bar{k}_1+\bar{k}_2$) for the 420–90°D run. The solid lines are calculated values by the Monte Carlo simulation.

Fig. 6 shows the π° energy calculated from the non-reconstructed energies of the two decay photons and the reconstructed π° energy for the 420–90°D run. The energy spread of the reconstructed π° meson was improved to be 70 MeV compared with the original spread of 160 MeV (FWHM). The energy resolution of the π° meson was estimated to be 4% (FWHM) by the Monte Carlo simulation.

The four momentum vector of the recoil nucleon, $(E_{nf}, \vec{p}_{nf})$, was determined by the TOF and the address of the nucleon hodoscope.

Since the most of published photoproduction cross sections are quoted as a function of the laboratory energy in the coordinate system where the target nucleons are at rest and the pion production angle in the c.m.s, we introduce the equivalent effective laboratory energy k^R and the π° production angle $\theta^c_{\pi^\circ}$ in the γn center of mass system. The total energy $\sqrt{s}$ is a proper variable in comparison with the reaction $\gamma p \to \pi^\circ p$ from free protons. Using four momentum vectors $(E_{\pi^\circ}, \vec{p}_{\pi^\circ})$ and $(E_{nf}, \vec{p}_{nf})$ of a π° meson and a recoil nucleon, the total energy squared s is given by

$$s=(E_{\pi^\circ}+E_{nf})^2+(\vec{p}_{\pi^\circ}+\vec{p}_{nf})^2. \tag{13}$$

The equivalent incident photon energy in the target-at-rest system is

$$k^R=(s-m^2)/2m, \tag{14}$$

where m is the nucleon on-shell mass. The π° production angle in the γN c.m. is obtained as follows:

$$\cos\theta^c_{\pi^\circ} = \frac{E^c_{\pi^\circ}}{p^c_{4^\circ}}\left[1 - \frac{kE_{\pi^\circ}}{k^c E^c_{\pi^\circ}}\left(1 - \frac{p_{\pi^\circ}}{E_{\pi^\circ}}\cos\theta_{\pi^\circ}\right)\right] \tag{15}$$

with $E^c_{\pi^\circ} = (s + m^2_{\pi^\circ} - m^2)/2\sqrt{s}$,

where the upper suffix denotes the center of mass system.

The four momentum vector of the initial target nucleon was also obtained from the energy-momentum conservation:

$$k + E_{ni} = E_{\pi^\circ} + E_{nf}, \tag{16a}$$

$$\vec{k} + \vec{p}_{ni} = \vec{p}_{\pi^\circ} + \vec{p}_{nf}, \tag{16b}$$

where $(k, \vec{k})$, $(E_{ni}, \vec{p}_{ni})$, $(E_{\pi^\circ}, \vec{p}_{\pi^\circ})$ and $(E_{nf}, \vec{p}_{nf})$ are the four momentum vectors of the incident photon, initial target nucleon, π° meson and the recoil nucleon, respectively.

The validity of the kinematical reconstruction was checked the results on the reaction $\gamma p \to \pi^\circ p$ on a free proton target.

III–3. Corrections

The background from the empty target was less than 12%. The background due to the accidental coincidence between π° mesons and recoil nucleons amounted to be 8–30% for the reaction (1) and 2–15% for the reaction (2).

The energy loss of protons in the target was appreciably large for the low photon energies and forward π° angles runs. The loss of protons was 8% for the 335–90° run and 26% for the 335–70° run.

The accidental coincidence rate of γ-veto counters was negligibly small and less than 1%.

The background from double pion production was estimated to be negligibly small because that the end-point energy of the bremsstrahlung spectrum was set about 180 MeV higher than the photon energy to corresponding to the central energy of the acceptance of the detection system.

III–4. Monte Carlo Simulation

The reduction of the cross sections for the reaction (1) and (2) from the measured counting rate was very complicated because of the complex functions of the detection efficiencies of the π° meson and nucleon with many independent variables and because of the smearing effect due to the Fermi motion of nucleons in the deuterium target. The detection efficiency and acceptance were evaluated by a Monte Carlo method assuming that the spectator model is valid for the bound nucleon.

The experimental coincidence yield of the π° meson and recoil nucleon from the deuterium target is given by

$$Y(k^R) = \iint \frac{d\sigma}{d\Omega^c_{\pi^\circ}}(k^R, \theta^c_{\pi^\circ})d\Omega^c_{\pi^\circ} \cdot N(k)dk \cdot N_T \cdot \phi(p_{ni})d^3p_{ni} \times T(\vec{x}_\perp)\eta(\vec{p}_{\pi^\circ}, \vec{p}_{nf}, \vec{x})d^3x, \tag{17}$$

where $Y(k^R)$: experimental coincidence yield of the π° meson and recoil nucleon per MU.

$\frac{d\sigma}{d\Omega^c_{\pi^\circ}}(k^R, \theta^c_{\pi^\circ})$: differential cross section for the reaction (1) and (2) depending on

the incident photon energy k^R in the target-at-rest system and the π° c.m. angle $\theta^c_{\pi^\circ}$.

$N(k)\mathrm{d}k$: number of photons per MU in the energy interval $\mathrm{d}k$.

N_T: number of target nucleons.

$\phi(p_{ni})$: initial nucleon momentum distribution.

$T(\vec{x}_\perp)$: normalized spatial intensity function of the incident photons at the point $\vec{x}_\perp=(x_t, y_t)$ in the perpendicular plane to the photon axis.

$\eta(\vec{p}_{\pi^\circ}, \vec{p}_{nf}, \vec{x})$: detection efficiency of the π° meson with momentum $\vec{p}_{\pi^\circ}$ and the recoil nucleon with momentum $\vec{p}_{nf}$ in coincidence produced at the target point $\vec{x}=(x_t, y_t, z_t)$, where z_t is the distance from the target center in the direction of the photon beam.

Eq. (17) involves a ninefold integration over kinematical and geometrical variables which depend on each other in a quite complicated way. In order to extract the cross sections, the following quantity must be calculated from the Monte Carlo simulation:

$$Y_M(k^R)=\iint \mathrm{d}\Omega^c_{\pi^\circ}\cdot N_M(k)\mathrm{d}k\cdot N_T\cdot\phi(p_{ni})\mathrm{d}^3p_{ni}\cdot T(x_\perp) \times\eta(\vec{p}_{\pi^\circ}, \vec{p}_{nf}, \vec{x})\mathrm{d}^3x/C, \tag{18}$$

where $N_M(k)\mathrm{d}k$: number of photons generated by random number in the Monte Carlo simulation.

C: correction factor for the integral region of the π° production angle in the c.m.s. and the decay photon angle from the π° meson in the rest system.

Finally the differential cross sections can be expressed from eqs. (17) and (18) as follows:

$$\frac{\mathrm{d}\sigma}{\mathrm{d}\Omega^c_{\pi^\circ}}(k^R, \theta^c_{\pi^\circ})=\frac{Y(k^R)}{Y_M(k^R)}\Big/C\frac{\int N(k)\mathrm{d}k}{\int N_M(k)\mathrm{d}k} =\frac{Y(k^R)}{Y_M(k^R)}\Big/\frac{C}{M}Q\int\frac{B(k)}{k}\mathrm{d}k, \tag{19}$$

where $M=\int N_M(k)\mathrm{d}k$: number of trial events in the Monte Carlo simulation.

The flow chart of the Monte Carlo simulation is shown in Fig. 7. Events are generated simulation reactions (1) and (2) under the following conditions:

a) The energy spectrum $N(k)$ of the bremsstrahlung photon beam is calculated by the Schiff's thin-target formula (Fig. 4).

b) The spatial intensity function $T(\vec{x}_\perp)$ of the incident photons has the Gaussian distribution with the standard deviation of 1.0 cm. The interaction takes place inside the target with uniform probability along the beam axis. In reconstruction of the four momentum vectors of the π° meson and the recoil nucleon, the reaction point is chosen to be the center of the target.

c) The target nucleon has the momentum distribution of the Hulthèn wave function for the dueteron ground state:

$$\phi(p_{ni})=\frac{4\alpha\beta(\alpha+\beta)}{\pi(\beta-\alpha)^2}\left(\frac{p^2_{ni}}{p^2_{ni}+\alpha^2}-\frac{p^2_{ni}}{p^2_{ni}+\beta^2}\right)^2, \tag{20}$$

where $\alpha=46.03$ MeV/c, $\beta=285.5$ MeV/c and p_{ni} is the initial nucleon momentum (i.e. the spectator nucleon momentum) in MeV/c.

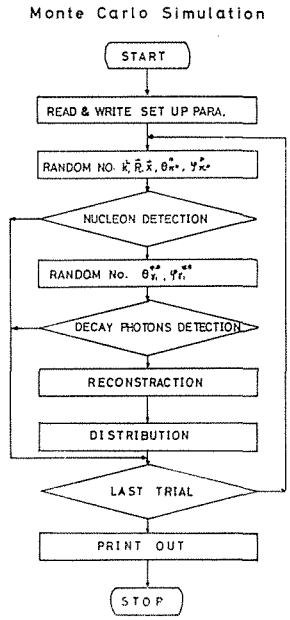

Fig. 7. Flow chart of the Monte Carlo simulation.

d) The π° production angle $\theta^c_{\pi^\circ}$, $\psi^c_{\pi^\circ}$ in the c.m.s. and the decay photon angle θ'_1, ψ'_1 in the π° rest system are assumed to be isotropic. In order to achieve a high efficiency of the Monte Carlo simulation, we limit the integral region of the angles of the π° meson and the decay photon.

e) The detection efficiency consists of the following parts:

$$\eta(\vec{p}_{\pi^\circ}, \vec{p}_{nf}, \vec{x}) = \eta_g(\vec{p}_{\pi^\circ}, \vec{p}_{nf}, \vec{x}) \cdot \eta_{\pi^\circ}(\vec{p}_{\pi^\circ}, \vec{x}) \cdot \eta_n(T_{nf}) \tag{21}$$

$$\eta_{\pi^\circ}(\vec{p}_{\pi^\circ}, \vec{x}) = \prod_{i=1}^{2} \eta_{\mathrm{LiH}}(k_i) \cdot \eta_{\mathrm{conv}}(k_i) \cdot \eta_C(k_i, \vec{X}_i) \tag{22}$$

where

$\eta_g(\vec{p}_{\pi^\circ}, \vec{p}_{nf}, \vec{x})$: geometrical detection efficiency of the coincidence events between the π° meson and recoil nucleon.

$\eta_n(T_{nf})$: detection efficiency of the nucleon hodoscope for the recoil neutron with the kinetic energy of T_{nf}.

$\eta_{\mathrm{LiH}}(k_i)$: attenuation factor of the LiH hardener for photons.

$\eta_{\mathrm{conv}}(k_i)$: conversion efficiency of photons for the lead converter.

$\eta_C(k_i, \vec{X}_i)$: detection efficiency of the Čerenkov counter for the photon with incident position $\vec{X}_i$.

(i) The conversion efficiency of photons into electron-positron pairs is given by

$$\eta_{\mathrm{conv}}(k) = 1 - e^{-\mu x} \tag{23}$$

$$\mu = \sigma_{\mathrm{pair}}(k) \rho N / A, \tag{24}$$

where k: incident photon energy.

x: thickness of the lead converter.

p: density of lead.

N: Avogadro number.
A: mass number of lead.
σ_{pair}: total pair cross section.

The conversion efficiency for the lead converter of $1X_0$ and $2X_0$ are calculated from the total cross sections given by A. Sørenssen[21] and T. Miyachi *et al*[22].

(ii) The pulse height spectra of the Čerenkov counters are the Gaussian type with measured energy resolution. Edge effects, i.e. the dependence of the pulse height on the incident position of the decay photon, are taken into account.

(iii) The time spectrum of the recoil nucleon is the Gaussian distribution with the resolution of 1 ns (FWHM). The energy loss of the recoil nucleon in the target, the lead absorber and the neutron veto counter is folded.

(iv) The angular resolution of the two dimensional hodoscope and the nucleon hodoscope are taken into account.

All the simulated events thus generated were also reconstructed using the same procedure for the real events. In order to test the validity of the above procedure, we compared quantities which did not depend on the dynamics of the reaction. They should be identical for the real and simulated events. Some examples of this comparison are shown in Fig. 8 and 9 for the reaction $\gamma d \rightarrow \pi^\circ p(n_s)$ at the 420–90°D run. Any miscalculation of the scattered momenta of the π° meson and recoil nucleon should be directly reflected into the only completely unmeasured quantity, the initial

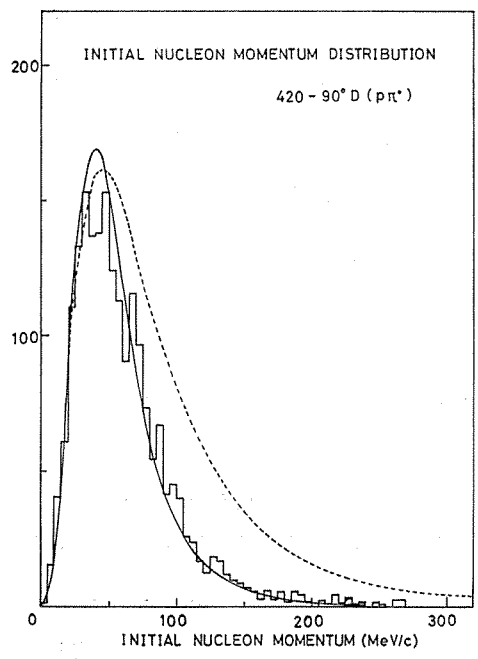

Fig. 8. Comparison between real events (histogram) and Monte Carlo events (solid line) for the neutron spectator momentum distribution at the 420–90°D run. The dashed line shows the calculated values from the Halthèn wave function for the deuteron.

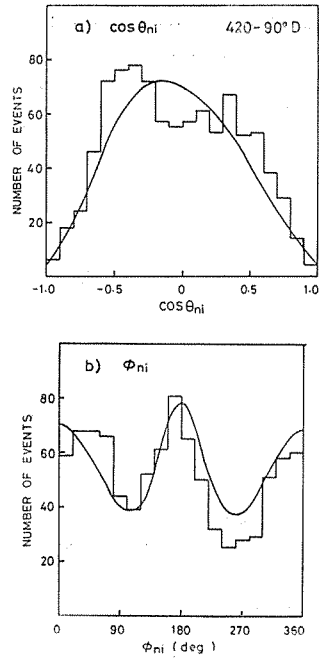

Fig. 9. Angular distribution of the neutron spectator for the 420–90°D run. a) polar angle $\cos\theta_{ni}$ b) azimuthal angle ϕ_{ni}. The solid lines show the results from the Monte Carlo simulation.

nucleon momentum (*i.e.* the spectator nucleon momentum). The real and simulated events are in good agreement. The momentum distribution predicted from the Hulthèn wave function in eq. (20) is also shown. The high momentum spectators are strongly suppressed in the coincidence measurement of this experiment. This is important because high momentum spectators can be the result of the final state interactions. The angular distributions of the polar (θ_{ni}) and azimutal (ψ_{ni}) angles in the laboratory should be isotropic. The depopulation observable near 90° and 270° is due to instrumental inefficiencies. The present experimental set-up had the maximum efficiency for the events which occur in the horizontal plane, while the events initiated from the target nucleons having the vertical momenta were not detected with high efficiencies. This effect is equally observable in the real and simulated events. These make us confident that the Monte Carlo simulation is an adequate representation of the experimental conditions.

The energy resolution and the angular resolution were obtained as the difference between the initial and reconstructed values:

$$\Delta k^R = k^R - k'^R \tag{25}$$

$$\Delta\theta^c_{\pi^\circ} = \theta^c_{\pi^\circ} - \theta'^c_{\pi^\circ}\,, \tag{26}$$

where (k'^R, $\theta'^c_{\pi^\circ}$) and (k^R, $\theta^c_{\pi^\circ}$) are the initial and reconstructed values for the incident photon in the target-at-rest system and the π° c.m. angle, respectively. Fig. 10 shows the incident photon energy and π° c.m. angular distributions. The difference between the real and simulated events indicate that the cross sections decrease steeply in this energy region. The energy and angular acceptances and their resolutions for

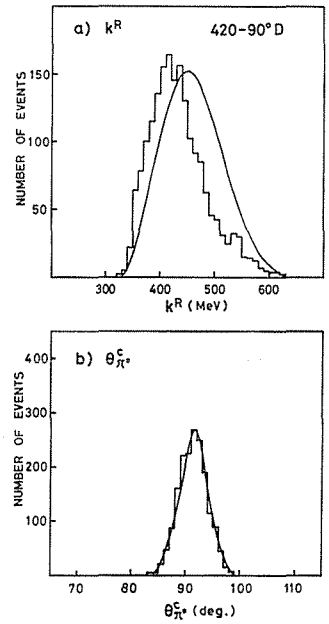

Fig. 10. Results of the kinematical reconstruction for the 420–90°D run. The solid lines are the calculated values by the Monte Carlo simulation. a) energy distribution of incident photons in the target-at-rest system. b) production angle distribution of π° mesons in the c.m. system.

Table 1. Energy and angular acceptances and their resolutions calculated from the Monte Carlo simulation.

Run (k-θ target)	$k^R \pm \delta k^R$ (MeV)	Δk^R (deg.)	$\theta^c_{\pi^\circ} \pm \delta\theta^c_{\pi^\circ}$ (deg.)	$\Delta\theta^c_{\pi^\circ}$ (deg.)
320– 70°D	335± 45	15	68±4	3.8
420– 70°D	455± 70	17	73±3.5	3.0
570– 70°D	717±106	20	73±3.5	2.8
300– 90°D	315± 38	15	89±3	3.5
420– 90°D	455± 70	17	92±3.5	3.5
570– 90°D	615±117	26	92±3	3.2
750– 90°D	810±146	40	91±3	2.8
350–110°D	375± 57	12	111±3.5	3.3
450–110°D	480± 85	25	111±3	3.3
570–110°D	610±110	38	111±4	3.3
375–130°D	395± 57	20	130±3	3.0
450–130°D	485± 90	28	130±3	2.6
570–130°D	615±120	38	130±3	2.5
300– 90°H	310± 35	13	88±3	3.8
420– 90°H	435± 61	15	91±3	3.0
570– 90°H	600±100	23	92±3	2.5

δk^R and $\delta\theta^c_{\pi^\circ}$ denote the energy and angular acceptances (FWHM). Δk^R and $\Delta\theta^c_{\pi^\circ}$ are the resolutions (FWHM) of the incident photon energy in the target-at-rest system and the π° c.m. angle, respectively.

each set-up parameter are listed in Table 1. For the 90°D runs, these quantities are also shown in Fig. 11. The energy acceptance was several times wider than the energy resolution so that data were divided by 4 to 5 energy bins for each experimental arrangement. The angular acceptance was nearly equal to its resolution for the most arrangement.

III–5. Reduction of the Cross Sections

The cross sections of π° production from a deuterium and hydrogen targets were obtained from eq. (19). In order to study the structures in the cross sections, the results were subdivided into smaller bins of the incident photon energy k^R. The

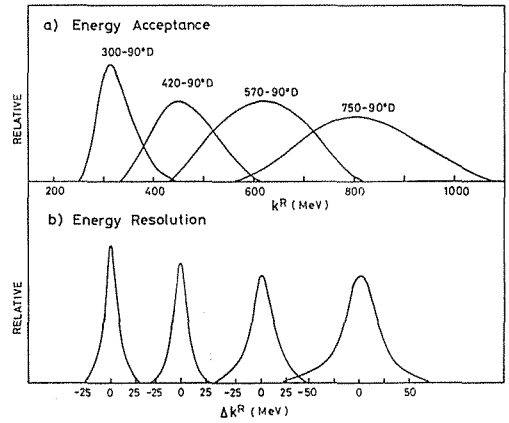

Fig. 11. Energy acceptance and energy resolution calculated by the Monte Carlo simulation for the 90°D runs.

choice of the bin size was dictated by the energy resolution and the minimum amount of statistics. In Fig. 11, there is a certain degree of overlap between the k^R spectra of adjacent incident energy settings; this allowed us to average results from different

Table 2. Measured differential cross sections for the reactions $\gamma d \to \pi^\circ n(p_s)$ and $\gamma d \to \pi^\circ p(n_s)$.

k^R (MeV)	$\theta^c_{\pi^\circ}$ (deg.)	$\frac{d\sigma}{d\Omega}(\gamma d \to \pi^\circ np_s)$ (μb/sr)	$\frac{d\sigma}{d\Omega}(\gamma d \to \pi^\circ pn_s)$ (μb/sr)
335±15	68.0±3.0	20.56±2.12	19.73±1.85
365±15	69.0±3.0	14.80±1.95	16.98±1.59
400±20	70.5±2.5	10.39±1.34	15.28±1.24
440±20	71.5±3.0	11.44±1.46	11.26±1.13
480±20	73.0±3.0	6.31±0.79	5.47±0.51
530±30	72.0±3.0	4.31±0.45	4.54±0.35
590±30	72.5±2.5	4.18±0.45	3.40±0.27
650±30	73.5±2.5	3.62±0.55	2.65±0.26
710±30	74.5±2.0	3.66±0.64	3.26±0.34
305±15	87.5±2.5	20.69±2.13	24.33±1.50
335±15	88.5±3.0	16.85±1.97	21.17±1.39
365±15	90.0±3.0	20.20±2.86	15.94±1.64
400±20	91.0±3.0	13.86±1.65	13.91±1.28
440±20	91.0±2.5	10.96±1.41	10.20±1.01
480±20	91.5±2.5	7.83±1.01	6.78±0.59
530±30	92.0±3.0	5.56±0.67	5.34±0.32
590±30	91.0±3.0	4.45±0.52	3.84±0.26
650±30	91.0±3.0	3.19±0.45	3.05±0.22
710±30	90.0±3.0	3.23±0.41	3.32±0.24
770±30	91.0±3.0	2.55±0.41	3.26±0.29
830±30	91.0±2.0	2.15±0.46	3.02±0.31
890±30	91.5±2.0	1.30±0.35	1.55±0.27
950±30	92.5±2.0	1.08±0.35	1.85±0.27
305±15	108.0±3.0	23.79±5.47	23.41±3.54
335±15	109.0±3.0	24.24±3.29	23.53±1.68
365±15	109.0±3.0	20.96±2.65	16.00±1.22
400±20	109.0±3.0	15.19±1.67	15.50±0.93
440±20	110.0±3.0	10.19±0.93	8.35±0.50
480±20	110.5±3.0	6.45±0.64	5.36±0.29
530±30	110.0±3.0	4.46±0.41	3.12±0.17
590±30	110.0±3.0	3.13±0.44	2.84±0.19
650±30	111.0±3.0	2.37±0.41	2.11±0.18
710±30	111.5±2.5	2.39±0.51	1.91±0.22
335±15	128.0±2.0	17.41±4.00	23.62±4.34
365±15	128.5±2.5	14.52±2.20	14.00±1.67
400±20	129.0±3.0	11.52±1.35	10.14±0.86
440±20	130.0±3.0	7.37±0.84	5.37±0.42
480±20	130.0±3.0	5.31±0.72	3.25±0.30
530±30	129.5±3.5	3.33±0.49	2.19±0.19
590±30	130.0±3.0	2.11±0.34	1.21±0.14
650±30	130.0±2.5	2.28±0.97	0.91±0.15
710±30	130.5±2.5	1.01±0.34	0.89±0.15

k^R is the incident photon energy and $\theta^c_{\pi^\circ}$ is the π° c.m. angle. The error includes the statistical deviations of the experiment and the Monte Carlo simulation.

energy settings. The low statistics tails of the k^R-distributions were cut out to obtain more reliable cross sections. The results were not subdivided into bins of the π° production angle $\theta^c_{\pi^\circ}$.

The results are listed in Table 2 for the reactions $\gamma d \to \pi^\circ n(p_s)$ and $\gamma d \to \pi^\circ p(n_s)$. These differential cross sections take into account the effect of the Fermi motion but ignore anything beyond the single scattering a) and a') diagrams in the next section.

The π° cross sections obtained with a hydrogen target are summarized in Table 3 and shown in Fig. 12, which were measured with the same detection system at 90° runs, in order to check the whole detection efficiency and the validity of the spectator model for a deuterium target. The data for the $\gamma p \to \pi^\circ p$ reaction shows good agreement with other experiments[23] and the theoretical fit from the phenomenological analyses of Moohouse, Oberlack and Rosenfeld (MOR),[24] and Metcalf and Walker (MW).[25] This makes us confident that the π° and recoil nucleon detectors are in normal operation and the Monte Carlo procedure is an adequate representation of

Table 3. Differential cross sections for the reaction $\gamma p \to \pi^\circ p$ using a hydrogen target. k is the incident photon energy and $\theta^c_{\pi^\circ}$ is the π° c.m. angle. The quoted error is staistical only.

k (MeV)	$\theta^c_{\pi^\circ}$ (deg.)	$\frac{d\sigma}{d\Omega}(\gamma p \to \pi^\circ p)$ (μb/sr)
305±15	88.0±2.0	26.38±1.69
335±15	88.5±2.0	29.37±1.91
365±15	90.0±2.0	21.62±2.26
400±20	90.0±1.5	16.00±1.01
440±20	91.0±1.5	11.16±0.72
480±20	91.5±1.5	6.30±0.74
530±30	90.0±1.5	4.99±0.39
590±30	91.0±1.5	3.50±0.27.
650±30	93.0±1.5	3.35±0.29
710±30	94.0±1.5	3.06±0.35

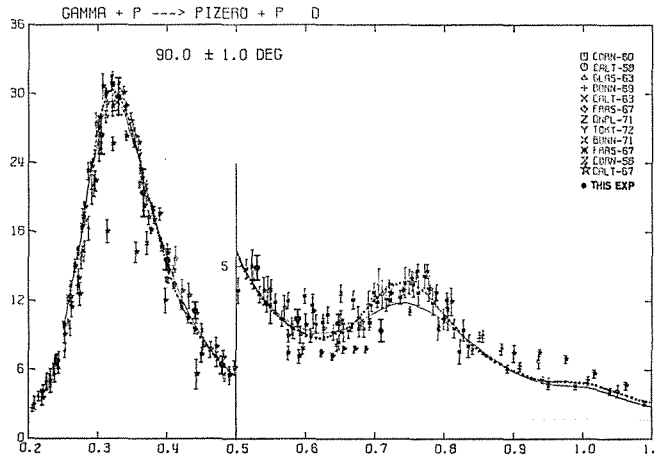

Fig. 12. Differential cross sections for the $\gamma p \to \pi^\circ p$ reaction as a function of the incident photon energy using a hydrogen target.

the experimental conditions.

IV. Deuteron Problems

It is impossible to study the reaction $\gamma n \to \pi^\circ n$ from a free neutron directly because of non-existence of a free neutron target. As a substitute for a neutron target, a deuterium target is used. The reaction under study takes place in a deuterium nucleus so that the final states recorded by experiment cannot be considered as due to a single interaction in a hydrogen target. In addition the interaction occurs on the nucleon which is not at rest and has a momentum distribution reflecting the deuteron wave function. In deuterium target experiments, the following effects must be generally taken into account:[13),26)]

a) smearing effect due to the Fermi motion of nucleons in deuterium,
b) multiple scattering and final state interaction,
c) the Glauber effect[27)] due to the shadowing of one nucleon by the other,
d) the Pauli exclusion principle and the Coulomb scatrering,
e) off-shell mass effect due to the nucleon and mesons in the intermediate states.

For the π° production the Pauli exclusion principle and the Coulomb scattering need not to be considered.

The problem of extracting cross sections on free neutrons from deuteron data is only partially understood at present. In high energies and small momentum transfers region, Glauber's theory of the multiple scattering expansion has been used with great success.[28)] In the first resonance $\Delta(1232)$ and large scattering angles region, however, its validity is doubtful for several reasons:

1) the large amplitude of the resonance may cause a very slow convergence of the multiple scattering series,
2) Glauber's theory is hold at the small angle scattering approximation,
3) the rapid variation of the amplitudes with the photon energy necessitates a more careful evaluation of the effect of the Fermi motion in the deuteron.

In order to investigate experimentally the deuteron effects the ratios between the cross sections from the $\gamma d \to \pi^\circ p(n_s)$ and $\gamma p \to \pi^\circ p$ reactions are needed:

$$R_{D/H} = \frac{d\sigma}{d\Omega}(\gamma d \to \pi^\circ p n_s) \Big/ \frac{d\sigma}{d\Omega}(\gamma p \to \pi^\circ p) . \tag{27}$$

Using the following factorization assumption,

$$R_{D/n} = \frac{d\sigma}{d\Omega}(\gamma d \to \pi^\circ n p_s) \Big/ \frac{d\sigma}{d\Omega}(\gamma n \to \pi^\circ n) \cong R_{D/H} \tag{28}$$

the cross sections for the $\gamma n \to \pi^\circ n$ reaction are deduced from the deuteron data:

$$\frac{d\sigma}{d\Omega}(\gamma n \to \pi^\circ n) \cong \frac{1}{R_{D/H}} \frac{d\sigma}{d\Omega}(\gamma d \to \pi^\circ p n_s) \tag{29a}$$

$$= R \frac{d\sigma}{d\Omega}(\gamma p \to \pi^\circ p) , \tag{29b}$$

where $$R = \frac{d\sigma}{d\Omega}(\gamma d \to \pi^\circ n p_s) \Big/ \frac{d\sigma}{d\Omega}(\gamma d \to \pi^\circ p n_s) .$$

The factorization assumption seems to be a good approximation because the deuteron

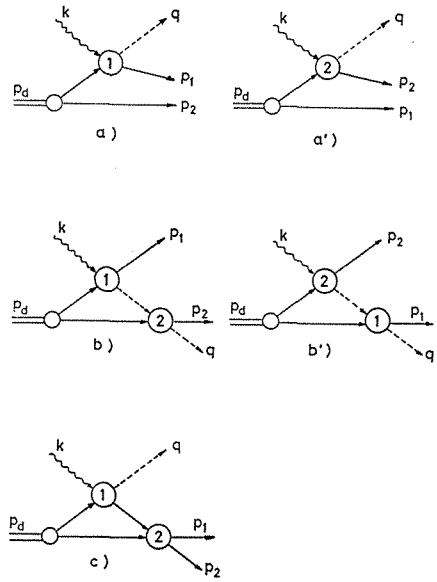

Fig. 13. Feynman diagrams of the three main effects in the $\gamma d \to \pi^\circ NN_s$ reaction studied in this experiment. a) and a'), b) and b'), and c) denote the single-scattering, the double-scattering and the final state interaction, respectively.

effects are cancelled out from the charge symmetric pair of final states $\pi^\circ np_s$ and $\pi^\circ pn_s$. Strictly speaking this factorization property is already violated in the first order the impulse approximation, due to the presence of interference terms between the single-scattering diagrams a) and a') in Fig. 13. In higher orders of the impulse approximation, the multiple scattering terms b) and b') also violate the factorization.

The detail studies on the deuteron effects are needed especially at our energy region. Therefore, following the model given by Julius,[13] we have made an evaluation of the ratio $R_{D/H}$ for the π° and π^+ production and made a comparison with experimental results including our results of the ratio $R_{D/H}$. Then, we obtained the differential cross sections from the present measurements on the reaction $\gamma n \to \pi^\circ n$ using our deuteron correction factor of $R_{D/n}$.

IV–1. Formalism

In a formal scattering theory, a Hamiltonian operator for the system consisting of an incident particle and two interacting nucleons in a deuterium target can be written in the form

$$H = H_0 + V, \tag{30}$$

where

$$H_0 = K_p + K_1 + K_2 + U,$$
$$V = V_1 + V_2. \tag{31}$$

Here K_p and K_α ($\alpha = 1, 2$) are the kinetic energy operators for the projectile particle and the α-th target nucleon; U is the deuteron binding potential; and V_α represents the interaction of the projectile with the α-th target nucleon. The transition operator

for interactions of the projectile with the bound nucleon α is given by the Lippmann-Schwinger equation:

$$\begin{aligned} t_\alpha &= V_\alpha + V_\alpha g t_\alpha = V_\alpha (1 - g V_\alpha)^{-1}, \\ g &= 1/(E_i - K_p - K_1 - K_2 - U + i\varepsilon), \end{aligned} \tag{32}$$

where g is the propagator and $E_i = k + E_d$ is the energy of the initial state. For interaction of the projectile with both target nucleons, the transition operator is similarly described as follows;

$$\mathscr{T}_d = (V_1 + V_2)[1 - g(V_1 + V_2)]^{-1}. \tag{33}$$

Using the operator identity

$$\frac{1}{1-a-b} = \frac{1}{1-a} + \frac{1}{1-a} b \left[\frac{1}{1-a} + \frac{1}{1-a} b \right] \frac{1}{1-a} + \cdots \tag{34}$$

eq. (33) is equivalent to

$$\mathscr{T}_d = t_1 + t_1 g t_2 + t_1 g t_2 g t_1 + \cdots + (1 \leftrightarrow 2). \tag{35}$$

This is the multiple scattering expansion. The term t_α corresponds to the single-scattering a) or a') and the term $t_\alpha g t_\beta$ ($\alpha \neq \beta = 1, 2$) represents the double-scattering b) or b') or the final state interaction c) in Fig. 13. The intermediate meson or nucleon correspond to the propagator g. Higher order terms are referred to as triple-scattering and so on.

On the other hand, the transition operator for interaction of the projectile with a free target nucleon can be written as follows corresponding to eqs. (32) and (33):

$$\begin{aligned} \mathscr{T}_\alpha &= V_\alpha + V_\alpha g_f \mathscr{T}_\alpha = V_\alpha (1 - g_f V_\alpha)^{-1}, \\ g_f &= 1/(k + E_\alpha - K_p - K_\alpha + i\varepsilon). \end{aligned} \tag{36}$$

The scattering operators t_α in the multiple scattering expansion (35) represent interactions with bound nucleons (as can be seen by the presence of the deuteron binding potential U in eq. (32). Therefore, in general, it is very difficult to calculate for an interacting three body system. Let us now introduce the following assumptions in order to calculate the multiple scattering expansion as simply as possible.

a) The impulse approximation[29] is valid. This approximation depends on two assumptions i) the incident particle interacts with only one nucleon at a time and ii) the interacting nucleon acts as if it were free, i.e. effects of the deuteron binding potential can be neglected for the duration of the collision. This approximation is expected to be good for interactions at high energies where the interaction time is short compared with the period of the nucleon system and the nucleon interaction cross sections are not large compared with the geometric cross section of deuteron. The transition operator t_α can be written approximately from eqs. (37) to (41),

$$t_\alpha \simeq \mathscr{T}_\alpha, \tag{37}$$

and eq. (35) can be rewritten as

$$\mathscr{T}_d \simeq \mathscr{T}_1 + \mathscr{T}_1 (E_i - K_p - K_1 - K_2 + i\varepsilon)^{-1} \mathscr{T}_2 + \cdots + (1 \leftrightarrow 2). \tag{38}$$

b) The off-shell effects due to the nucleon and meson in the intermediate states is assumed to be small. Using a theorem of generalized function theory, the propagator g assuming that $U \simeq 0$ is written as

$$(E_i-K_p-K_1-K_2+i\varepsilon)^{-1}=\frac{P}{E_i-K_p-K_1-K_2} -i\pi\delta(E_i-K_p-K_1-K_2), \qquad (39)$$

where P denotes the Cauchy principal value. The principal value term corresponds to off energy shell propagation in the intermediate state. The δ-function term, when inserted in eq. (38), implies the energy conservation between the initial and intermediate states. The principal value term is assumed to be small compared with the δ-function term so that eq. (38) is written approximately as

$$\mathscr{T}_d\simeq\mathscr{T}_1-i\pi\mathscr{T}_1\delta(E_i-K_p-K_1-K_2)\mathscr{T}_2+\cdots+(1\leftrightarrow2). \qquad (40)$$

c) We consider five low order Feynman diagrams in the multiple scattering expansion, which are shown in Fig. 13. Finally the multiple scattering expansion takes the form

$$\mathscr{T}_d\simeq\mathscr{T}_1+\mathscr{T}_2-i\pi[\mathscr{T}_1\delta(E_i-K_p-K_1-K_2)\mathscr{T}_2 +\mathscr{T}_2\delta(E_i-K_p-K_1-K_2)\mathscr{T}_1]. \qquad (41)$$

The single-scattering diagrams a) and a') correspond to $\mathscr{T}_1$ and $\mathscr{T}_2$, respectively. The double-scattering diagram b) and the final state interaction diagram c) correspond to $-i\pi\mathscr{T}_2\delta(E_i-K_p-K_1-K_2)\mathscr{T}_1$ and the diagram b') corresponds to $-i\pi\mathscr{T}_1\cdot\delta(E_i-K_p-K_1-K_2)\mathscr{T}_2$.

The cross section for the reaction

$$\gamma(k)+\mathrm{d}(p_d)\rightarrow\pi^\circ(q)+N_1(p_1)+N_2(p_2) \qquad (42)$$

is described by

$$\sigma=\frac{1}{4F}|M_{fi}|^2\mathrm{d}Lips(s;\,Q,\,P_1,\,P_2),$$
$$\mathrm{d}Lips(s;\,Q,\,P_1,\,P_2)=(2\pi)^4\delta^4(P_f-P_i)\frac{1}{(2\pi)^9}\frac{\mathrm{d}^3q}{2E_{\pi^\circ}}\frac{\mathrm{d}^3p_1}{2E_1}\frac{\mathrm{d}^3p_2}{2E_2}, \qquad (43)$$

where M_{fi} is an invariant matrix element and F is Møller's invariant flux factor, $F=kE_dv$. v is relative velocity between initial particles, $v=\left|\frac{\vec{k}}{E_\gamma}-\frac{\vec{P}_d}{E_d}\right|$. $\mathrm{d}Lips(s;\,Q,\,P_1,\,P_2)$ is 3-body Lorentz invariant phase space with final four momenta Q, P_1 and P_2. The transition matrix element in eq. (41) is defined as

$$\mathscr{T}_d=(2\pi)^{-9/2}(2k\cdot2E_d\cdot2E_{\pi^\circ}\cdot2E_1\cdot2E_2)^{-1/2}M_{fi}, \qquad (44)$$

so that the cross section (43) is written as follows:

$$\sigma=\frac{(2\pi)^4}{v}\int\mathrm{d}^3q\mathrm{d}^3p_1\mathrm{d}^3p_2|\mathscr{T}_d|^2\delta^4(Q+P_1+P_2-K-P_d). \qquad (45)$$

The differential cross section measured by the coincidence method for the reaction (42) in the lab. system ($\vec{p}_d=0$) is given by

$$\frac{\mathrm{d}\sigma}{\mathrm{d}\Omega_{\pi^\circ}\mathrm{d}^3p_1}=(2\pi)^4\int q^2\mathrm{d}q\mathrm{d}^3p_2\delta(E_{\pi^\circ}+E_1+E_2-k-m_d) \times\delta^3(\vec{q}+\vec{p}_1+\vec{p}_2-\vec{k})<q,\,p_1,\,p_2|\mathscr{T}_d|k,\,p_d=0,\,\Omega_d>|^2$$
$$=(2\pi)^4qE_{\pi^\circ}|<q,\,p_1p_2|T_d|k,\,p_d=0,\,\Omega_d>|^2, \qquad (46)$$

where m_d is the deuteron mass; $|\Omega_d>$ denotes the deuteron state, $|\Omega_d> = |p_d, \Omega, v, \xi>$ and $|v, \xi>$ is the spin-isospin state. Ω is the deuteron radial wave function written by the S and D state wave functions

$$\Omega(\vec{r}) = \frac{1}{\sqrt{4\pi}\, r}\left[u(r) + \frac{1}{\sqrt{8}} S_{12} w(r)\right] \tag{47}$$

with normalization

$$\int_0^\infty dr[u^2(r) + w^2(r)] = 1, \tag{48}$$

and S_{12} is the tensor operator

$$S_{12} = \frac{3}{r^2}\vec{\sigma}(1)\cdot\vec{r}\vec{\sigma}(2)\cdot\vec{r} - \vec{\sigma}(1)\cdot\vec{\sigma}(2)\,, \tag{49}$$

where $\vec{\sigma}(\alpha)$ is the Pauli spin operator for the α-th nucleon. The deuteron wave function in the momentum space becomes

$$\hat{\Omega}(p) = \frac{1}{(2\pi)^{3/2}}\int \mathrm{d}^3 r e^{i\vec{p}\cdot\vec{r}}\, \Omega(\vec{r})$$
$$= \hat{u}(p) - \frac{1}{\sqrt{8}} S_{12}\hat{w}(p)\,, \tag{50}$$

$$\begin{Bmatrix} \hat{u}(p) \\ \hat{w}(p) \end{Bmatrix} = \frac{1}{\sqrt{2\pi}}\int_0^\infty r\mathrm{d}r \begin{Bmatrix} j_0(pr)u(r) \\ j_2(pr)w(r) \end{Bmatrix} \tag{51}$$

where $j_i(pr)$ is the i-th order spherical Bessel function.

a) Single-scattering

The single-scattering contribution to the matrix element in eq. (45) from the Feynman diagram a) is written by

$$\langle q, p_1, p_2 | \mathscr{T}_1 | k, p_d = 0, \Omega_d\rangle = \int \mathrm{d}^3 p_1' \mathrm{d}^3 p_2' \langle q, p_1, p_2 | \mathscr{T}_1 | p_1', p_2'\rangle$$
$$\times \langle p_1', p_2' | p_d = 0, \Omega_d\rangle$$
$$= \langle q, p_1, p_2 | T_1 | k, -p_2\rangle \hat{\Omega}(\vec{p}_2), \tag{52}$$

where $\vec{p}_2 = \vec{k} - \vec{q} - \vec{p}_1$. In deriving this eq., we used

$$\langle q, p_1, p_2 | \mathscr{T}_1 | p_1', p_2'\rangle$$
$$= \delta^3(\vec{q} + \vec{p}_1 - \vec{k} - \vec{p}_1')\delta^3(\vec{p}_2' - \vec{p}_2)\langle q, p_1 | T_1 | k, p_1'\rangle \tag{53}$$

and

$$\langle p_1', p_2' | p_d = 0, \Omega_d\rangle = \delta^3(\vec{p}_1' + \vec{p}_2')\hat{\Omega}\left(\frac{\vec{p}_1' - \vec{p}_2'}{2}\right). \tag{54}$$

Similarly, the contribution from the diagram a') is

$$\langle q, p_1, p_2 | \mathscr{T}_2 | k, p_d = 0, \Omega_d\rangle$$
$$= \langle q, p_2 = k - q - p_2 | T_2 | k, -p_1\rangle \hat{\Omega}(\vec{p}_1)\,. \tag{55}$$

If we choose the Hulthèn wave function for the deuteron state,

$$\hat{\Omega}(\vec{p})=\hat{u}(p)=\frac{\sqrt{\alpha\beta(\alpha+\beta)^3}}{\pi}\frac{1}{(p^2+\alpha^2)(p^2+\beta^2)} \tag{56}$$

then we find that the contribution from a') as compared with a) is depressed by the factor

$$\frac{\hat{\Omega}(p_1)}{\hat{\Omega}(p_2)}=\frac{(p_2^2+\alpha^2)(p_1+\beta^2)}{(p_1^2+\alpha^2)(p_1+\beta^2)}\lesssim 0.042 \tag{57}$$

for $p_1\gtrsim 250$ MeV/c and $p_2\simeq 50$ MeV/c. The recoil nucleon momentum is always larger than 250 MeV/c in any set-up condition of this experiment. The spectators with the momentum larger than 100 MeV/c are strongly suppressed in the coincidence measurement compared with the momentum distribution calculated from the Hulthèn wave function as shown in Fig. 8. Therefore we shall disregard the contribution from the diagram a').

b) Double-scattering

Since, in the low energy region of the present experiment, the γN interactions are dominated by the first resonance there is a strong resonance in the πN system. Therefore, the double-scattering effects represented by the diagrams b) and b') in Fig. 13 must be taken into account. This means that the Glauber's shadowing effect of one nucleon on the other are also taken into account of the calculation. First, we consider the diagram b) representing large angle production of the intermediate π meson at the first step, followed by forward scattering at the second step. From eq. (41) this amplitude is given by

$$\begin{aligned}
&-i\pi\langle q,\, p_1,\, p_2|\mathscr{T}_2\delta(k+m_d-k_p-k_1-k_2)\mathscr{T}_1|k,\, p_d=0,\, \Omega_d\rangle\\
&=-i\pi\sum_x\int \mathrm{d}^3q_x\mathrm{d}^3p_1''\mathrm{d}^3p_2''\mathrm{d}^3p_2'\mathrm{d}^3p_2'\langle q,\, p_1,\, p_2|\mathscr{T}_2|q_x,\, p_1'',\, p_2''\rangle\\
&\quad\times\delta(k+m_d-E_x(q_x)-E_1(p_1'')-E_2(p_2''))\langle q_k,\, p_1'',\, p_2''|\mathscr{T}_1|k,\, p_1',\, p_2'\rangle\\
&\quad\times\langle p_1',\, p_2'|p_d=0,\, \Omega_d\rangle\,,
\end{aligned} \tag{58}$$

where $|q_x,\, p_1'',\, p_2''>$ and $|p_1',\, p_2'>$ denote a (xnp) state and a non-interacting two nucleon state. x is the intermediate mesons. Integrating over the δ-functions contained in the definitions of the matrix elements as in eq. (53), we obtain the contribution to the matrix element in eq. (46):

$$\begin{aligned}
&-i\pi\langle q,\, p_1,\, p_2|\mathscr{T}_2\delta(k+m_d-k_p-k_1-k_2)\mathscr{T}_1|k,\, p_d=0,\, \Omega_d\rangle\\
&=-i\pi\sum_x\int d^3p\langle q,\, p_2=k-q-p_1|T_2|q_x=k+p-p_1,\, -p\rangle\\
&\quad\times\langle q_x=k+p-p_1,\, p_1|T_1|k,\, p\rangle\delta(k+m_d-E_x(q_x)\\
&\qquad\qquad -E_1(p_1)-E_2'(p))\hat{\Omega}(\vec{p})\,.
\end{aligned} \tag{59}$$

Second, the contribution from the diagram b') representing forward π production in the first interaction and large angle scattering of π mesons in the second collision, is similarly given by

$$\begin{aligned}
&-i\pi\langle q,\, p_1,\, p_2|\mathscr{T}_1\delta(k+m_d-K_p-K_1-K_2)\mathscr{T}_2|k,\, p_d=0,\, \Omega_d\rangle\\
&=-i\pi\sum_x\int d^3p\langle q,\, p_1|T_1|q_x=q+p_1-p,\, p\rangle\\
&\qquad\times\langle q_x=q+p_1-p,\, p_2=k-q-p_1|T_2|k,\, -p\rangle\\
&\times\delta(k+m_d-E_x(q_x)-E_1'(p)-E_2(p_2))\hat{\Omega}(\vec{p})\,.
\end{aligned} \tag{60}$$

c) Final State Interaction

The correction arising from the final state interaction between nucleons is taken into account to the single-scattering term a) and neglected to the double-scattering terms. This diagram represents large angle scattering of the intermediate nucleon in the first interaction, followed by forward production in the second interaction. The contribution of the final state interaction amplitude to the matrix element in eq. (46) is given in the same way as the double-scattering case:

$$\begin{aligned}
&-i\pi\langle q,\ p_1,\ p_2|\mathscr{T}_2\delta(k+m_d-k_p-k_1-k_2)\mathscr{T}_1|k,\ p_d=0,\ \Omega_d\rangle \\
&=-i\pi\int d^3p\langle p_1,\ p_2=k-q-p_1|T_2^{NN}|P_N=k+p-q,\ -p\rangle \\
&\qquad\times\langle q,\ p_N=k+p-q|T_1|k,\ q\rangle \\
&\qquad\times\delta(k+m_d-E_{\pi^\circ}(q)-E_N(q_N)-E_2'(p))\hat{\Omega}(\vec{p}), \qquad (61)
\end{aligned}$$

where T_2^{NN} is the nucleon-nucleon scattering amplitude and E_N and P_N are the intermediate nucleon energy and momentum, respectively.

Let us now introduce the following simplified notation for the reaction $x(k)+N_\alpha(p)\to y(q)+N_\alpha(p_f)$ $(\alpha=1, 2)$:

$$T_\alpha^{xN}(k,\ \Delta)\equiv\langle q,\ p_f|T_\alpha|k,\ p\rangle, \qquad (62)$$

where $\vec{\Delta}=\vec{k}-\vec{p}$ is three momentum transfer. Using this notation, the total amplitude is written from eqs. (52), (59), (60) and (61) in the following form:

$$\begin{aligned}
T_d&=T_1^{\gamma N}(k,\ \Delta)\hat{\Omega}(\vec{p}_2) \\
&\quad-i\pi\sum_x\int d^3pT_2^{\pi N}(q+p_2+p,\ p_2+p)T_1^{\gamma N}(k,\ \Delta-p_2-p) \\
&\qquad\times\delta(k+m_d-E_x(q+p_2+p)-E_1(\Delta-p_2)-E_2'(p))\hat{\Omega}(\vec{p}) \\
&\quad-i\pi\sum_x\int d^3pT_1^{\pi N}(k-p-p_2,\ \Delta-p-p_2)T_2^{\gamma N}(k,\ p+p_2) \\
&\qquad\times\delta(k+m_d-E_x(k-p-p_2)-E_2(p_2))\hat{\Omega}(\vec{p}) \\
&\quad-i\pi\int d^3pT_2^{NN}(\Delta+p,\ p_2+p)T_1^{\gamma N}(k,\ \Delta) \\
&\qquad\times\delta(E_1(\Delta-p_2)+E_2(p_2)-E_N(\Delta+p)-E_2'(p))\hat{\Omega}(\vec{p}). \qquad (63)
\end{aligned}$$

In order to evaluate the integrals in eq. (63) we set spectator momentum $\vec{p}_2=0$ and assume that each amplitude is almost unchanged in the small integral region of the internal nucleon momentum p and the final state π° meson momentum q is large compared with p. The π° meson momentum was larger than 200 MeV/c in this experiment. In addition, we adopt the following procedure of expanding the various particle energies in the internal nucleon momentum p and retain only the linear terms:[30]

$$\begin{aligned}
&\int d^3p\delta(k+m_d-E_x(q+p)-E_1(\Delta)-E_2'(p))\,\hat{\Omega}(\vec{p}) \\
&=\frac{E_x(q)}{q}\int d^2p_{\perp q}\hat{\Omega}(p_{\parallel q},\ \vec{p}_{\perp q})\simeq\lambda\frac{E_x(q)}{q}, \qquad (64)
\end{aligned}$$

$$\begin{aligned}
&\int d^3p\delta(k+m_d-E_x(k-p)-E_1(\Delta)-E_2'(p))\,\hat{\Omega}(\vec{p}) \\
&=\frac{E_x(k)}{k}\int d^2p_{\perp k}\hat{\Omega}(p_{\parallel k},\ \vec{p}_{\perp k})\simeq\lambda\frac{E_x(k)}{k} \qquad (65)
\end{aligned}$$

and
$$\int \mathrm{d}^3p\,\delta(E_1(\Delta)+m_2-E_N(\Delta+p)-E_2'(p))\hat{\Omega}(\vec{p})$$
$$=\frac{E_N(\Delta)}{\Delta}\int \mathrm{d}^2p_{\perp\Delta}\hat{\Omega}(p_{\parallel\Delta},\ \vec{p}_{\perp\Delta})\simeq\lambda\frac{E_N(\Delta)}{\Delta} \tag{66}$$

with
$$\lambda\equiv\int \mathrm{d}^2p\hat{\Omega}(0,\ \vec{p})=2\sqrt{2\pi}\int_0^\infty \mathrm{d}z\,\Omega(z)\,, \tag{67}$$

where $\vec{p}\equiv(p_{\parallel e},\ \vec{p}_{\perp e})$ and $\vec{e}$ denotes any vector; $p_{\parallel x}$ is the component of $\vec{p}$ parallel to $\vec{e}$; $\vec{p}_{\perp e}$ is the vector of $\vec{p}$ perpendicular to $\vec{e}$.

Finally the total amplitude (63) can be rewritten in the simple form:

$$\begin{aligned}T_d\simeq{}&T_1^{\gamma N}(k,\ \Delta)\hat{\Omega}(0)\\&-i\pi\lambda\Big[\sum_x\frac{E_x(q)}{q}\,T_2^{\pi N}(q,\ 0)T_1^{\gamma N}(k,\ \Delta)\\&+\sum_x\frac{E_x(k)}{k}\,T_1^{\pi N}(k,\ \Delta)T_2^{\gamma N}(k,\ 0)\\&+\frac{E_N(\Delta)}{\Delta}\,T_2^{NN}(\Delta,\ 0)\ T_1^{\gamma N}(k,\ \Delta)\Big],\end{aligned} \tag{68}$$

where $\hat{\Omega}(0)=3.536\ (\mathrm{fm})^{3/2}$ and $\lambda=1.770\ (\mathrm{fm})^{-1/2}$ for the Hulthèn wave function.

In order to obtain the differential cross section, the total amplitude T_d must be sandwiched between spin and isospin functions for the initial and final two nucleons states. For simplification of the spin and isospin procedure, we adopt now the closure approximation in the summation over all final N–N states. The N–N states having high effective masses and being not accessible by energy conservation are also included in principle, but the contribution from the forbidden high mass states to the sum over all states is very small because the matrix element is large only when the kinematics correspond to the recoil nucleon with momentum $\vec{\Delta}$. Here it should be noted that the contribution from the final state interaction in the diagram c) could be included in the closure approximation. The differential cross section can be thus described from eq. (41) using the completeness of the final N–N states as follows:

$$\begin{aligned}\frac{\mathrm{d}\sigma}{\mathrm{d}\Omega_{\pi^\circ}\mathrm{d}^3p_1}&=(2\pi)^4qE_{\pi^\circ}\sum_{\nu,\xi}\langle\nu,\ \xi|T_d^\dagger\ T_d|\nu,\ \xi\rangle\\&=(2\pi)^4\,qE_{\pi^\circ}\sum_{\nu,\xi}<\nu,\ \xi\Big|\,\hat{\Omega}^2(0)T_1^{\dagger\gamma N}(k,\ \Delta)T_1^{\gamma N}(k,\ \Delta)\\&\quad+2\pi\lambda\hat{\Omega}((0)\,\mathrm{Im}\Big[\sum_x\frac{E_x(q)}{q}\,T_1^{\dagger\gamma N}(k,\ \Delta)T_2^{\pi N}(q,\ 0)\ T_1^{\gamma N}(k,\ \Delta)\\&\quad+\sum_x\frac{E_x(k)}{k}\,T_1^{\dagger\gamma N}(k,\ \Delta)T_1^{\pi N}(k,\ \Delta)T_2^{\gamma N}(k,\ 0)\Big]\Big|\nu,\ \xi>\,,\end{aligned} \tag{69}$$

where $|\nu,\ \xi>$ denotes the initial deuteron spin-isospin state. Here we neglect the higher small terms, for example, $(T_2^{\pi N}T_1^{\gamma N})^\dagger(T_2^{\pi N}T_1^{\gamma N})$.

The amplitudes for the reactions $\gamma\mathrm{N}\to\pi\mathrm{N}$ and $\pi\mathrm{N}\to\pi\mathrm{N}$ are, in general, decomposed into the spin non-flip and flip amplitudes:

$$T_\alpha^{\gamma N}=A_\alpha+\vec{B}_\alpha\cdot\vec{\sigma}(\alpha)\,, \tag{70}$$

$$T_\alpha^{\pi N}=F_\alpha+\vec{G}_\alpha\cdot\vec{\sigma}(\alpha)\,, \tag{71}$$

where A_α and F_α are pure spin non-flip amplitudes and $\vec{B}_\sigma$ contains spin flip and non-flip parts. $\vec{G}_\alpha$ is a pure spin flip amplitude. For the unpolarized deuteron, the relevant expectation values have the form

$$\langle M \rangle \equiv \frac{1}{3} \sum_\nu \langle \nu | M | \nu \rangle , \tag{72}$$

where M is an operator and $|\nu>$ is the deuteron spin triplet state. Using the following results

$$\langle \vec{\sigma}(\alpha) \rangle = 0 \tag{73}$$

and $$\langle \vec{\sigma}_i(\alpha) \cdot \vec{\alpha}_j(\beta) \rangle = \frac{1}{3} \sigma_{ij} \qquad (\alpha \neq \beta),$$

the differential cross section for the unpolarized photon beam and deuteron target is rewritten from eq. (69) as

$$\begin{aligned} \frac{d\alpha}{d\Omega_{\pi^\circ} d^3 p_1} = (2\pi^4 q E_{\pi^\circ} \Big(& \hat{\Omega}^2(0)(|A_1(^2 + |\vec{B}_1|^2) \\ & + 2\pi\lambda \hat{\Omega}(0) \operatorname{Im} \Big[\sum_x \frac{E_x(q)}{q} \Big\{ (|A_1|^2 + |\vec{B}_1|^2) F_2 \\ & + \frac{1}{3} (A_1^* \vec{B}_1 \cdot \vec{G}_2) \Big\} + \sum_x \frac{E_x(k)}{k} \Big\{ \Big(A_1^* A_2 + \frac{1}{3} \vec{B}_1^* \cdot \vec{B}_2 \Big) F_1 \\ & + \Big(A_2 \vec{B}_1^* + \frac{1}{3} A_1^* \vec{B}_2 \Big) \cdot \vec{G}_1 \Big\} \Big] \Big) . \end{aligned} \tag{74}$$

The first term is reduced to the familiar form

$$\begin{aligned} \frac{d\sigma}{d\Omega_{\pi^\circ}} &= (2\pi)^4 q E_{\pi^\circ} (|A_1|^2 + |\vec{B}_1|^2) \int d^3 p_1 \hat{\Omega}(0) \\ &= (2\pi)^4 q E_{\pi^\circ} (|A_1|^2 + \vec{B}_1|^2) \int d^3 p_2 \hat{\Omega}(\vec{p}_2) \\ &= (2\pi)^4 q E_{\pi^\circ} (|A_1|^2 + |\vec{B}_1|^2) = \frac{d\sigma}{d\Omega_{\pi^\circ}} (\gamma N \to \pi^\circ N) \end{aligned} \tag{75}$$

in the absence of the Fermi motion. Here $d\sigma/d\Omega(\gamma N \to \pi^\circ N)$ is the differential cross section on a free nucleon target.

Then we obtain the deuteron correction (i.e. the ratio between the cross sections from the deuteron and free nucleon targets) as follows:

$$\begin{aligned} R_{D/n,H} = 1 + \frac{2\pi\lambda}{\hat{\Omega}(0)} \operatorname{Im} \Bigg[\sum_x \frac{E_x(q)}{q} \Bigg\{ F_2 + \frac{\frac{1}{3}(A_1^* \vec{B}_1 + A_1 \vec{B}_1^*)}{|A_1|^2 + |\vec{B}_1|^2} \vec{G}_2 \Bigg\} \\ + \sum_x \frac{E_x(k)}{k} \Bigg\{ \frac{A_1^* A_2 + \frac{1}{3} \vec{B}_1^* \vec{B}_2}{|A_1|^2 + |\vec{B}_1|^2} F_1 + \frac{A_2 \vec{B}_1^* + \frac{1}{3} A_1^* \vec{B}_2}{|A_1|^2 + \vec{B}_1|^2} \vec{G}_1 \Bigg\} \Bigg] . \end{aligned} \tag{76}$$

IV–2. Results of the Deuteron Corrections

For the calculation of the deuteron correction factor, we have used the MOR amplitudes[24] for the $\gamma N \to \pi N$ reactions and the phase shifts of CERN theoretical

fit[31] for the $\pi N \to \pi N$ reactions. The γN amplitudes A_α and $\vec{B}_\alpha$ and the πN amplitudes F_α and $\vec{G}_\alpha$ are derived from the MOR partial wave amplitudes and the phase shifts as described in Appendices A and B, respectively.

We summed over the intermediate pion states x allowed by isospin conservation. For the reaction $\gamma d \to \pi^\circ p(n_s)$, the allowed intermediate states x are π° and π^- mesons for the diagram b) and π^+ and π° mesons for the diagram b'). For the $\gamma d \to \pi^\circ n(p_s)$ reaction, the π° and π^+ meson states and the π^- and π° meson states are allowed for the diagrams b) and b'), respectively. The calculated deuteron correction factors $R_{D/H}$ and $R_{D/n}$ are shown in Figs. 14 and 15 and the numerical values are listed in

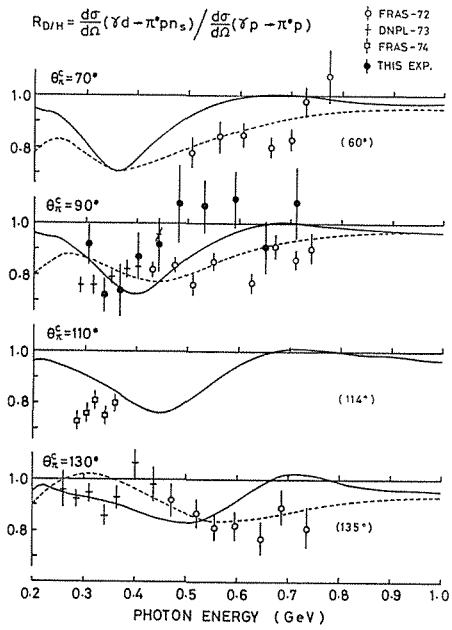

Fig. 14

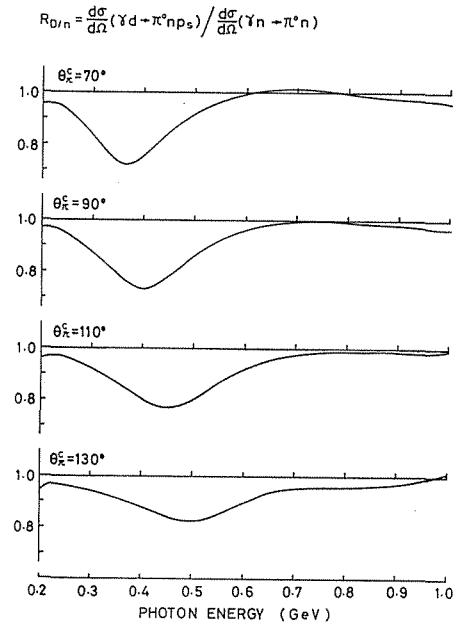

Fig. 15

Fig. 14. Cross section ratio $R_{D/H} = \frac{d\sigma}{d\Omega}(\gamma d \to \pi^\circ p n_s) / \frac{d\sigma}{d\Omega}(\gamma p \to \pi^\circ p)$ as a function of incident photon energy. The solid curves are predicted from this model. The dashed curves are calculated by Baldini-Celio and Sciacca[32].

Fig. 15. Cross section ratio $R_{D/n} = \frac{d\sigma}{d\Omega}(\gamma d \to \pi^\circ n p_s) / \frac{d\sigma}{d\Omega}(\gamma n \to \pi^\circ n)$ predicted from this model.

Table 4. The experimental data are also plotted in Fig. 14 together with other data.[10-12] Theoretical prediction curves (dashed lines) by Baldini-Celio and Sciacca[32] are also shown. In addition, we compared with the ratio between π^+ production cross sections on deuterium and hydrogen targets.

$$R^+_{D/H} = \frac{d\sigma}{d\Omega}(\gamma d \to \pi^+ n n_s) \Big/ \frac{d\sigma}{d\Omega}(\gamma p \to \pi^+ n) \tag{77}$$

by Fujii *et al.*[33] in order to test the validity of the model, as shown in Fig. 16. The dash-dotted curves in Fig. 16 are calculated by the lowest order impulse approximation with closure.[34-35] The results of this simple spectator model agree with the data at small production angles but disagree at large angles. In the first resonance region,

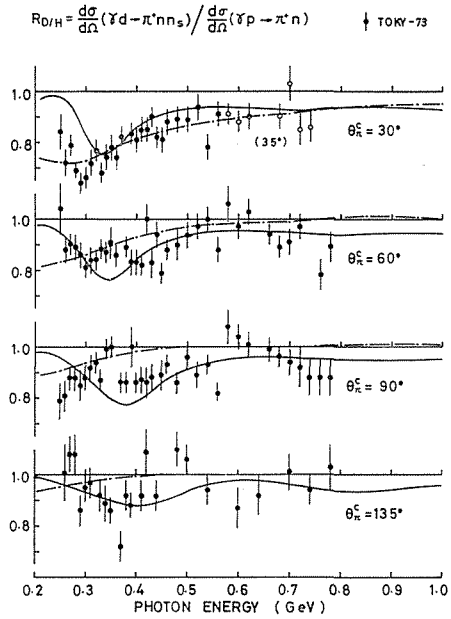

Fig. 16. Cross section ratio $R^+_{D/H} = \frac{d\sigma}{d\Omega}(\gamma d \to \pi^+ n n_s) / \frac{d\sigma}{d\Omega}(\gamma p \to \pi^+ n)$ by T. Fujii *et al.*[83] The solid curves are predictions from this model. The dash-dotted curves are calculated by Chew and Lewis[84].

the data seems to show dip structure due to the double-scattering (*i.e.* pion rescattering) effects which is reproduced well with the present calculation. It should be noted that for $\pi^\pm$ production the deuteron corrections due to the Pauli exclusion effect and the final state interaction are also important besides the double-scattering process. On the other hand, for π° production the double-scattering effects are relatively large because of absence of the Pauli exclusion effect and of the large cross sections for the reactions $\pi^+ p \to \pi^+ p$ and $\pi^- n \to \pi^- n$ around the first resonance region. Therefore, the double-scattering effects which is neglected in the simple spectator model are important for π° production in the first resonance region.[36]

In the energy region above 0.5 GeV, the present calculation shows small corrections due to the double-scattering effect corresponding to smaller cross section of πN scattering. Therefore, our prediction and the measured ratio of $R_{D/H}$ for π° production give larger values than the experimental results at Frascati[10] and are almost unity.

These results show that the deuteron corrections other than smearing effect can exceed 20% in the first resonance region at small angles. We adopted the Hulthèn wave function for the deuteron state. The difference due to choice of the Hulthèn and Gartenhause wave functions was within 6%. The present calculation including the effects of double-scattering reproduces well the experimental results on $R_{D/H}$ for both π^+ and π° productions. The calculated values of $R_{D/H}$ and $R_{D/n}$ in Table 4 indicate that the factorization assumption in eq. (28) is good in the over all energy region except in the second resonance region at 130° and about 7%. This is due to the contribution from the double-scattering diagram b') in Fig. 13 and indicates that the isoscalar amplitude is appreciable in the second resonance region.

V. Results and Discussions

V–1. Differential Cross sections

The smearing effect due to the Fermi motion was taken into account in reduction of the cross section for the reactions (1) and (2), so that the cross sections $\gamma n \rightarrow \pi^{\circ} n$

Table 4. Differential cross sections for the reactions $\gamma n \rightarrow \pi^{\circ} n$ and $\gamma p \rightarrow \pi^{\circ} p$ extracted from deuterium data and the deuteron correction factors. The quoted error is statistical only.

k^R (MeV)	$\theta^c_{\pi^{\circ}}$ (deg.)	$R_{D/n}$	$\frac{d\sigma}{d\Omega}(\gamma n \rightarrow \pi^{\circ} n)$ (μb/sr)	$R_{D/H}$	$\frac{d\sigma}{d\Omega}(\gamma p \rightarrow \pi^{\circ} p)$ (μb/sr)
335±15	68.0±3.0	0.743	27.67±2.85	0.731	26.99±2.53
365±15	69.0±3.0	0.714	20.73±2.73	0.707	24.02±2.25
400±20	70.5±2.5	0.756	13.74±1.77	0.753	20.29±1.89
440±20	71.5±3.0	0.834	13.72±1.75	0.832	13.53±1.36
480±20	73.0±3.0	0.896	7.04±0.88	0.894	6.12±0.57
530±30	72.0±3.0	0.947	4.55±0.48	0.946	4.80±0.37
590±30	72.5±2.5	0.988	4.23±0.45	0.986	3.45±0.27
650±30	73.5±2.5	1.011	3.58±0.54	1.003	2.64±0.26
710±30	74.5±2.0	1.017	3.60±0.63	1.000	3.26±0.34
305±15	87.5±2.5	0.870	25.39±2.61	0.860	30.33±1.87
335±15	88.5±3.0	0.817	22.68±2.65	0.806	28.96±1.90
365±15	90.0±3.0	0.760	28.29±4.01	0.750	22.55±2.32
400±20	91.0±3.0	0.730	18.33±2.18	0.725	18.47±1.70
440±20	91.0±2.5	0.767	13.14±1.69	0.766	12.26±1.21
480±20	91.5±2.5	0.833	8.74±1.13	0.835	7.48±0.66
530±30	92.0±3.0	0.904	5.87±0.71	0.909	5.64±0.34
590±30	91.0±3.0	0.957	4.50±0.52	0.965	3.89±0.26
650±30	91.0±3.0	0.987	3.16±0.45	0.994	3.04±0.22
710±30	90.0±3.0	0.998	3.18±0.40	1.000	3.32±0.24
770±30	91.0±3.0	0.995	2.54±0.41	0.992	3.29±0.29
830±30	91.0±2.0	0.989	2.17±0.47	0.984	3.08±0.32
890±30	91.5±2.0	0.983	1.32±0.32	0.976	1.59±0.18
950±30	92.5±2.0	0.977	1.10±0.36	0.967	1.91±0.28
305±15	108.0±3.0	0.913	26.02±5.99	0.906	25.84±3.92
335±15	109.0±3.0	0.881	27.51±3.73	0.874	26.92±1.92
365±15	109.0±3.0	0.845	24.80±3.14	0.839	19.07±1.43
400±20	109.0±3.0	0.796	19.08±2.10	0.789	19.64±1.17
440±20	110.0±3.0	0.765	13.32±1.22	0.762	10.96±0.66
480±20	110.5±3.0	0.778	8.29±0.82	0.780	6.87±0.37
530±30	110.0±3.0	0.841	5.30±0.49	0.851	3.67±0.20
590±30	110.0±3.0	0.914	3.42±0.48	0.933	3.04±0.20
650±30	111.0±3.0	0.958	2.47±0.43	0.988	2.14±0.18
710±30	111.5±2.5	0.976	2.45±0.52	1.010	1.89±0.22
335±15	128.0±2.0	0.921	18.90±4.34	0.918	25.73±4.73
365±15	128.5±2.5	0.903	16.08±2.44	0.902	15.52±1.85
400±20	129.0±3.0	0.881	13.08±1.53	0.881	11.51±0.98
440±20	130.0±3.0	0.851	8.66±0.99	0.852	6.30±0.49
480±20	130.0±3.0	0.831	6.39±0.87	0.832	3.91±0.36
530±30	129.5±3.5	0.838	3.97±0.58	0.842	2.60±0.22
590±30	130.0±3.0	0.885	2.38±0.38	0.903	1.33±0.16
650±30	130.0±2.5	0.932	2.45±1.04	0.984	0.92±0.15
710±30	130.5±2.5	0.951	1.06±0.36	1.027	0.87±0.15

and $\gamma p \to \pi^\circ p$ for free nucleons were obtained from multiplying the deuterium data by the calculated correction factors $R_{D/n}^{-1}$ and $R_{D/H}^{-1}$, respectively. The corrected differential cross sections are summarized in Table 4. The energy and angular dependences of the cross sections were shown in Figs. 17–18 and Fig. 19, respectively. Other laboratories data[23),9-10),37)] are also plotted for comparison. The errors attached to this data are statistical only due to the counting yields and the Monte Carlo simulations. Sources of the systematic errors in the cross sections are listed in Table 5. The quadrature sum of the systematic errors was found to be 8%.

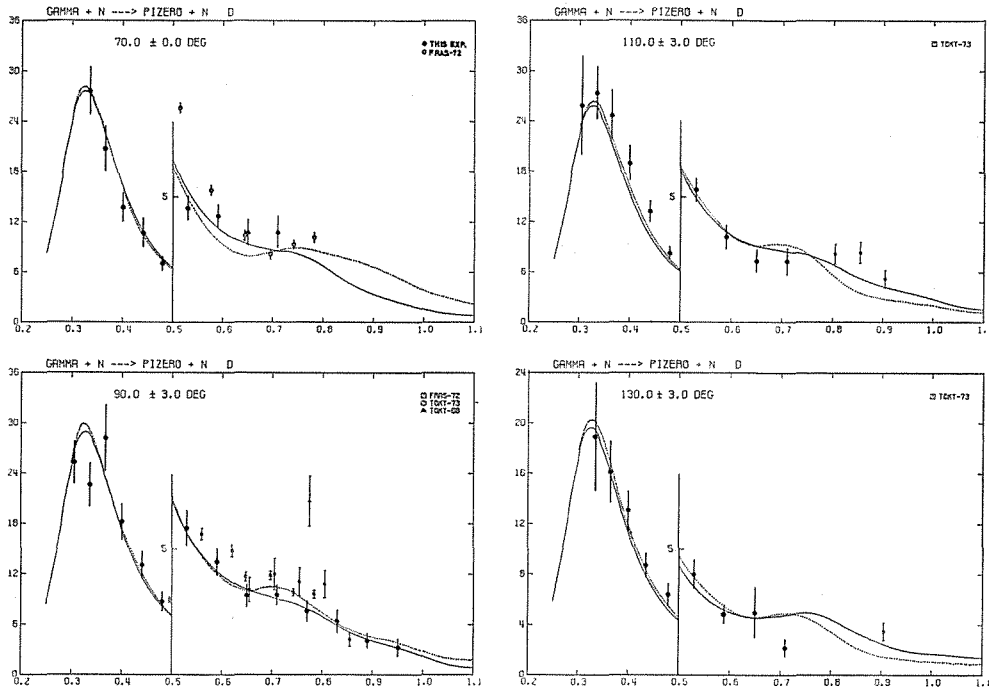

(a) (b)

Fig. 17. Differential cross sections $d\sigma/d\Omega(\gamma n \to \pi^\circ n)(\mu b/sr)$ as a function of the incident photon energy k^R (GeV). The solid curve is the prediction from the phenomenological analysis of MOR[24)] and the dotted curve from that of MW[25)]. ● this experiment, FRAS–72[10)], TOKY–73[9)] and TOKY–68[37)]. a) $\theta_{\pi^\circ}^c = 70°$ and 90°, b) $\theta_{\pi^\circ}^c = 110°$ ad 130°.

Table 5. Systematic errors.

Source of the systematic errors	Uncertainty
Beam intensity of bremsstrahlung photons	3 %
End-point energy of the beam spectrum	0.5%
Target density and length	1 %
Photon detection efficiency	1 %
Recoil nucleon detection efficiency	5 %
Conversion efficiency	3 %
Photon absorption	2 %
Effective acceptance	5 %
Deuteron correction	6 %
Quadrature sum	8 %

V–2. Discussions

The measured differential cross sections for the reaction $\gamma p \to \pi^\circ p$ from hydrogen and from deuterium are shown in Fig. 12 and Fig. 18a) and are in good agreement with the data obtained at other laboratories.[23] This makes us confident that the reduction procedure of the cross sections and the deuteron correction are appropriate.

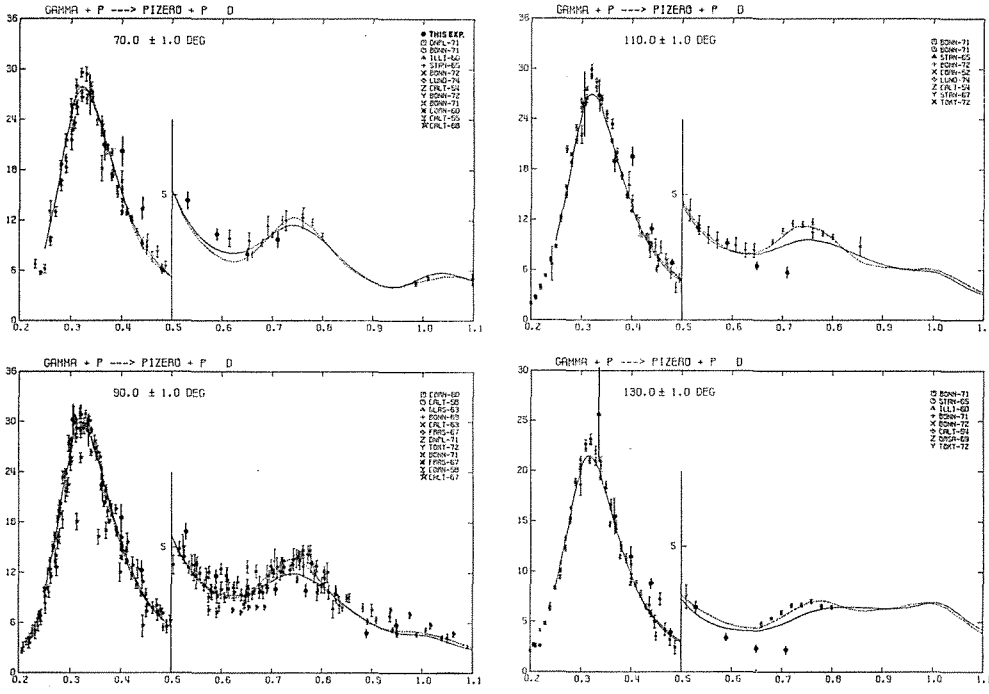

(a) (b)

Fig. 18. Differential cross sections $d\sigma/d\Omega(\gamma p \to \pi^\circ p)(\mu b/sr)$ as a function of the incident photon energy k^R (GeV). The curves are the same as in Fig. 17. a) $\theta^c_{\pi^\circ} = 70°$ and 90°, b) $\theta^c_{\pi^\circ} = 110°$ and 130°.

The results on the differential cross sections for the reactions $\gamma n \to \pi^\circ n$ and $\gamma p \to \pi^\circ p$ have a similar structure as shown in Figs. 17 and 18. The cross sections for both reactions show two peaks at the same energy 300 MeV and 700 MeV. The first peak is, as known well, due to the excitation of the $\Delta(1232)P_{33}$ resonance and the second peak is due to the $N(1520)D_{13}$ resonance. The cross sections for the reaction $\gamma n \to \pi^\circ n$ is somewhat larger than those for the reaction $\gamma p \to \pi^\circ p$ in the energy range 400 MeV to 710 MeV. This means that the isoscalar part has an appreciable contribution in the photoproduction amplitude.

In Figs. 17–19 the predictions from the two phenomenological analyses by Moorhouse, Oberlak and Rosenfeld (MOR)[24] and Metcalf and Walker (MW)[25] are also plotted by the solid and dotted curves, respectively. These analyses are based on the recent compilation of cross section and polarization data of single pion photoproduction with the exception of the reaction $\gamma n \to \pi^\circ n$. The present data is in good

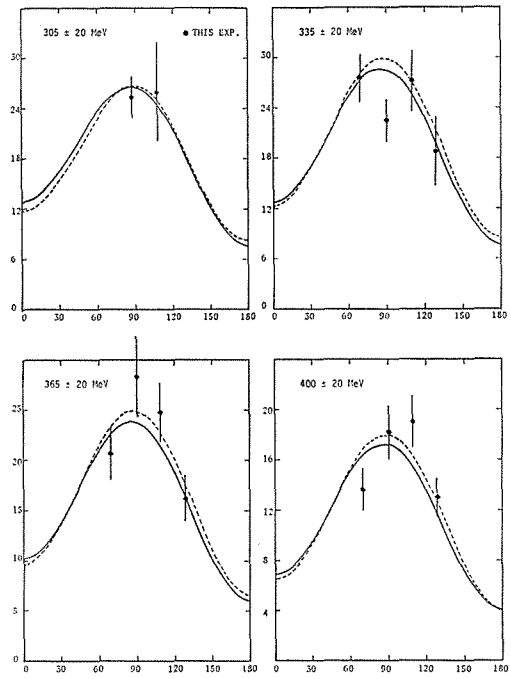
305 ± 20 MeV
● THIS EXP.
335 ± 20 MeV
365 ± 20 MeV
400 ± 20 MeV

(a)

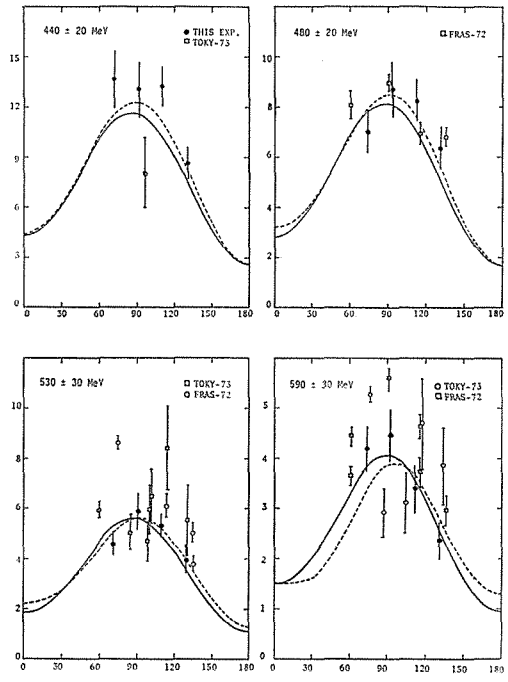
440 ± 20 MeV
● THIS EXP.
□ TOKY-73
480 ± 20 MeV
□ FRAS-72
530 ± 30 MeV
□ TOKY-73
○ FRAS-72
590 ± 30 MeV
○ TOKY-73
□ FRAS-72

(b)

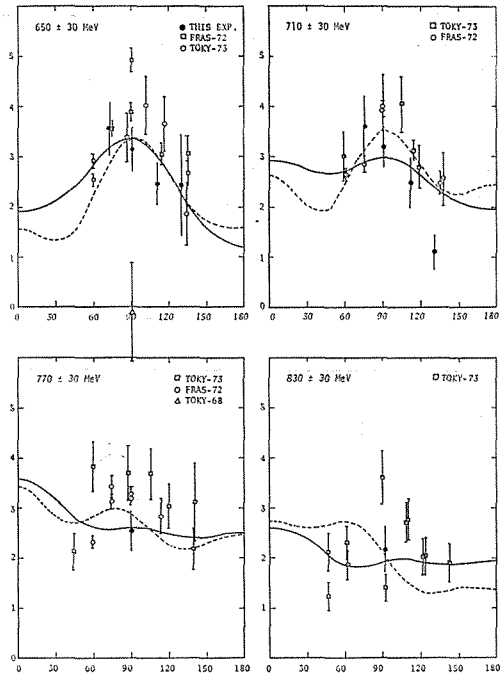

(c)

Fig. 19. The angular dependences of the differential cross sections for the reaction $\gamma n \to \pi^\circ n$. The curves are the same as in Fig. 17. a) $k^R = 305$, 335, 365 and 400 MeV, b) $k^R = 440$, 480, 530 and 590 MeV. c) $k^R = 650$, 710, 770 and 830 MeV.

agreement with the predictions from the MOR and MW analyses in the over all energy region.

If an isotensor term of I=2 exists in addition to the ordinary isovector and isoscalar terms in the electromagnetic hadronic current, the relation between the cross sections from neutrons and protons at the $\Delta(1232)$ resonance is given by introducing the parameter x in refs. 14 and 15:

$$\frac{d\sigma}{d\Omega}(\gamma n \to \pi^\circ n) = (1+x)^2 \frac{d\sigma}{d\Omega}(\gamma p \to \pi^\circ p)\,, \tag{78}$$

$${}_3M^n_{1+} = (1+x)\,{}_3M^p_{1+}\,, \tag{79}$$

where ${}_3M^{n(p)}_{1+}$ is the magnetic dipole amplitude for a neutron (proton) target. Assuming that $x = -0.3$ as suggested by Sanda, Shaw and Donnachie,[14-15] the cross section from neutrons is expected to be $\sim 1/2$ of that from protons. The present data shows that both cross sections are the same sizes at the $\Delta(1232)$ resonance. We conclude there is no positive evidence for an isotensor electromagnetic current. This result is consistent with the $\pi^\circ n/\pi^\circ p$ ratio experiments at Daresbury[11] and Frascati.[12]

In the $N(1470)P_{11}$ resonance region, the present results show that there is no enhancement for the $\gamma n \to \pi^\circ n$ cross sections in contrast with the previous Frascati data.[10] This discrepancy is seem to be due to the different deuteron correction factors as shown in Fig. 14.

In conclusion we summarized as follows: 1) The deuteron correction to the

differential cross sections are about 20% in the $\Delta(1232)$ resonance region. 2) The double-scattering (pion-rescattering) effect is very important at the $\Delta(1232)$ resonance especially for π° production from deuterium. 3) The differential cross sections for $\gamma n \to \pi^\circ n$ are consistent with predictions from the MOR and MW analyses. 4) There is no enhancement of the cross section due to the $N(1470)P_{11}$ resonance. 5) No positive evidence for an isotensor electromagnetic current is found.

Appendix A $\gamma N \to \pi N$ Amplitude

The CGLN amplitude for single pion photoproduction is written as

$$\begin{aligned}\mathscr{F} &= i\vec{\sigma}\cdot\vec{\varepsilon}\mathscr{F}_1 + \vec{\sigma}\cdot\hat{q}\vec{\sigma}\cdot(\hat{k}\times\vec{\varepsilon})\mathscr{F}_2 + i\vec{\sigma}\cdot\hat{k}\hat{q}\cdot\vec{\varepsilon}\mathscr{F}_3 + i\vec{\sigma}\cdot\hat{q}\hat{q}\cdot\vec{\varepsilon}\mathscr{F}_4 \\ &= \vec{\varepsilon}\cdot(\hat{q}\times\hat{k})\mathscr{F}_2 + i\vec{\sigma}\cdot[\vec{\varepsilon}\mathscr{F}_1 + (\hat{q}\cdot\vec{\varepsilon}\hat{k} - \hat{q}\cdot\hat{k}\vec{\varepsilon})\mathscr{F}_2 \\ &\quad + \hat{k}\hat{q}\cdot\vec{\varepsilon}\mathscr{F}_3 + \hat{q}\hat{q}\vec{\varepsilon}\mathscr{F}_4], \end{aligned} \tag{A.1}$$

where $\vec{\varepsilon}=(-\sin\phi, \cos\phi, 0)$ is the photon polarization vector, $\hat{q}=(\sin\theta, 0, \cos\theta)$ is the scattered pion unit vector with the scattering angle θ in the c.m.s. and $\hat{k}=(0, 0, 1)$ is the incident photon unit vector. The amplitudes being defined as eq. (75), a and $\vec{b}$ correspond to an invariant matrix element M_{fi} are

$$\begin{aligned} a &= -\cos\phi\sin\theta\,\mathscr{F}_2, \\ \vec{b} &= i[\vec{\varepsilon}(\mathscr{F}_1\cos\theta\mathscr{F}_2) + \hat{q}\cdot\vec{\varepsilon}\{\hat{k}(\mathscr{F}_2+\mathscr{F}_3) + \hat{q}\mathscr{F}_4\}]. \end{aligned} \tag{A.2}$$

Notice that averaged values over the photon polarization are

$$\langle M\sin^2\phi\rangle = \langle M\cos^2\phi\rangle = \frac{1}{2}M, \tag{A.3}$$

where M is some amplitude.

The relation between the CGLN amplitudes and the helicity amplitudes is given by

$$\begin{aligned} \mathscr{F}_1 &= -\frac{1}{2}\left[\frac{H_2-H_3}{\sqrt{2}\cos\frac{\theta}{2}} - \frac{H_4+H_1}{\sqrt{2}\sin\frac{\theta}{2}}\right], \\ \mathscr{F}_2 &= \frac{1}{2}\left[\frac{H_2-H_3}{\sqrt{2}\cos\frac{\theta}{2}} - \frac{H_4+H_1}{\sqrt{2}\sin\frac{\theta}{2}}\right], \\ \mathscr{F}_3 &= -\frac{1}{\sqrt{2}\sin\theta}\left[\frac{H_1}{\cos\frac{\theta}{2}} - \frac{H_3}{\sin\frac{\theta}{2}}\right], \\ \mathscr{F}_4 &= -\frac{1}{\sqrt{2}\sin\theta}\left[\frac{H_1}{\cos\frac{\theta}{2}} - \frac{H_3}{\sin\frac{\theta}{2}}\right], \end{aligned} \tag{A.4}$$

where $H_1 \equiv A_{1/2,3/2}$, $H_2 \equiv A_{1/2,1/2}$, $H_3 \equiv A_{-1/2,3/2}$ and $H_4 \equiv A_{-1/2,1/2}$. Here $A_{\mu\lambda}$ are helicity amplitudes with the initial and final state helicities $\lambda=\lambda_\gamma-\lambda_1$ and $\mu=-\lambda_2$. λ_γ, λ_1 and λ_2 are the incident photon, target nucleon and recoil nucleon helicities. The helicity amplitudes are expanded in terms of the partial waves $A_{l\pm}$ and $B_{l\pm}$ with $j=l\pm 1/2$ and parity $-(-)^l$ as follows:

$$
\begin{aligned}
H_1 &= \frac{1}{\sqrt{2}} \sin\theta \cos\frac{\theta}{2} \sum_{l=1}^{\infty} (B_{l+} - B_{(l+1)-})(P''_l - P''_{l+1}) , \\
H_2 &= \sqrt{2} \cos\frac{\theta}{2} \sum_{l=0}^{\infty} (A_{l+} - A_{(l+1)-})(P'_l - P'_{l+1}) , \\
H_3 &= \frac{1}{\sqrt{2}} \sin\theta \sin\frac{\theta}{2} \sum_{l=1}^{\infty} (B_{l+} + B_{(l+1)-})(P''_l + P''_{l+1}) , \\
H_4 &= \sqrt{2} \sin\frac{\theta}{2} \sum_{l=0}^{\infty} (A_{l+} + A_{(l+1)-})(P'_l + P'_{l+1}) ,
\end{aligned}
\tag{A.5}
$$

where l is the orbital angular momentum of the πN system and P'_l and P''_l are derivatives of Legendre polynomials.

The amplitudes for the reactions $\gamma p \to \pi^+ n$, $\gamma n \to \pi^- p$, $\gamma p \to \pi^\circ p$ and $\gamma n \to \pi^\circ n$ are decomposed in terms of the isoscalar and isovector amplitudes (assuming that there is no existence of the isotensor amplitude) as follows:

$$
\begin{aligned}
A(\gamma p \to \pi^+ n) &= -\sqrt{\frac{1}{3}} A^{V_3} + \sqrt{\frac{2}{3}} (A^{V_1} - A^S) , \\
A(\gamma n \to \pi^- p) &= \sqrt{\frac{1}{3}} A^{V_3} - \sqrt{\frac{2}{3}} (A^{V_1} + A^S) , \\
A(\gamma p \to \pi^\circ p) &= \sqrt{\frac{2}{3}} A^{V_3} + \sqrt{\frac{1}{3}} (A^{V_1} - A^S) , \\
A(\gamma n \to \pi^\circ n) &= \sqrt{\frac{2}{3}} A^{V_3} + \sqrt{\frac{1}{3}} (A^{V_1} + A^S) .
\end{aligned}
\tag{A.6}
$$

The amplitudes a, $\vec{b}$ for each reaction can be calculated from the partial waves $A_{l\pm}^{V_3, V_1, S}$ and $B_{l\pm}^{V_3, V_1, S}$ using eqs. (A.2), (A.4), (A.5) and (A.6).

The photoproduction cross section can be written as

$$
\frac{d\sigma}{d\Omega^*} = \frac{q^*}{k^*} (|a|^2 + |\vec{b}|^2) , \tag{A.7}
$$

where k^* and q^* are c.m. momenta of the incident photon and the pion, respectively. Using the amplitudes A and $\vec{B}$ correspond to the Lorentz non-invariant matrix element $T^{\gamma N}$, the cross section is also written as

$$
\frac{d\sigma}{d\Omega^*} = (2\pi)^4 \sqrt{\frac{k^* E^*_{Ni} E^*_\pi E^*_{N\,f}}{s}} \frac{q^*}{k^*} (|A|^2 + |\vec{B}|^2) , \tag{A.8}
$$

where $s = (k^* + E^*_{Ni})^2$ is total energy squared, E^*_π is the pion c.m. energy and $E^*_{Ni,f}$ are the nucleon c.m. energies in the initial and final states. The amplitudes A and $\vec{B}$ are given by

$$
A = \frac{1}{(2\pi)^2} \sqrt{\frac{s}{k^* E^*_{Ni} E^*_\pi E^*_{Nf}}}\, a \tag{A.9}
$$

and

$$
\vec{B} = \frac{1}{(2\pi)^2} \sqrt{\frac{s}{k^* E^*_{Ni} E^*_\pi E^*_{Nf}}}\, \vec{b}
$$

in the c.m. system.

Appendix B $\pi N \to \pi N$ Amplitude

The total isospin of the πN system is I=1/2 or 3/2 so that the amplitude for

each channel is decomposed into I=1/2 and I=3/2 amplitudes as follows:

$$\begin{aligned}
&T(\pi^+p\to\pi^+p) = T(\pi^-n\to\pi^-n) = \quad T_{3/2}\,,\\
&T(\pi^-p\to\pi^-p) = T(\pi^+n\to\pi^+n) = 2/3T_{1/2}+1/3T_{3/2}\,,\\
&T(\pi^-p\rightleftarrows\pi^\circ n) = T(\pi^+n\rightleftarrows\pi^\circ p) = -\sqrt{2}/3T_{1/2}+\sqrt{2}/3T_{3/2}\,,\\
&T(\pi^\circ p\to\pi^\circ p) = T(\pi^\circ n\to\pi^\circ n) = 1/3T_{1/2}+3/3T_{3/2}\,,
\end{aligned} \tag{B.1}$$

where $T_{1/2}$ and $T_{3/2}$ are the isospin I=1/2 and I=3/2 amplitudes.

The πN elastic amplitude is written by the spin non-flip and flip amplitudes as described in eq. (71):

$$M^{\pi N} = f(\theta) + g(\theta)\vec{\sigma}\cdot\vec{n}, \tag{B.2}$$

where θ is the pion scattering angle in the c.m.s. and $\vec{n} = \vec{p}_\pi^{\,*}\times\vec{q}_\pi^{\,*}/|\vec{p}_\pi^{\,*}\times\vec{q}_\pi^{\,*}|$ is the normal unit vector to the production plane ($\vec{p}_\pi^{\,*}$ and $\vec{q}_\pi^{\,*}$ are the initial and final pion moment).

The amplitudes $f(\theta)$ and $g(\theta)$ are expressed in term of partial waves by

$$\begin{aligned}
f^I(\Theta) &= \sum_{l=0}^{\infty}\,[(l+1)f^I_{l+}+lf^I_{l-}]\,P_l(\cos\theta)\,,\\
g^I(\Theta) &= \mathrm{i}\sum_{l=1}^{\infty}\,[f^I_{l+}-f^I_{l-}]\,P'_l(\cos\theta)\,,\\
f^I_{l\pm} &= \frac{1}{2iq_\pi}\,(\eta^I_{l\pm}\,e^{2i\delta^I_{l\pm}}-1)\,,
\end{aligned} \tag{B.3}$$

where $P_l(\cos\theta)$ are Legendre functions, $f^I_{l\pm}$ are the partial wave amplitudes for orbital angular momentum l and total angular momentum $j=l\pm1/2$, $\eta^I_{l\pm}$ are the elasticity and $\delta^I_{l\pm}$ are the phase shifts.

The differential cross section for πN elastic scattering can be written as

$$\frac{\mathrm{d}\sigma}{\mathrm{d}\Omega^*} = |f(\theta)|^2+|g(\theta)|^2 \tag{B.4}$$

in the c.m. system. Using the amplitudes F and $\vec{G}$ correspond to the Lorentz non-invariant matrix element $T^{\pi N}$, the cross section is also written as

$$\frac{\mathrm{d}\sigma}{\mathrm{d}\Omega^*} = (2\pi)^4\,\frac{E^*_{\pi i}E^*_{Ni}E^*_{\pi f}E^*_{Nf}}{s}\,\frac{q^*_\pi}{p^*_\pi}\,(|F|^2+|\vec{G}|^2)\,, \tag{B.5}$$

where $s=(E^*_{\pi i}+E^*_{Ni})^2$ is total energy squared and $E^*_{\pi i,f}$ and $E^*_{Ni,f}$ are the pion and nucleon c.m. energies in the initial and final states, respectively. From eq. (B.4) and (B.5) the amplitudes F and $\vec{G}$ are given by

$$\begin{aligned}
F &= \frac{1}{(2\pi)^2}\sqrt{\frac{s}{E^*_{\pi i}E^*_{Ni}E^*_{\pi f}E^*_{Nf}}}\;\sqrt{\frac{q^*}{p^*_\pi}}\,f(\theta)\\
\text{and}\qquad \vec{G} &= \frac{1}{(2\pi)^2}\sqrt{\frac{s}{E^*_{\pi i}E^*_{Ni}E^*_{\pi f}E^*_{Nf}}}\;\sqrt{\frac{q^*_\pi}{p^*_\pi}}\,g(\theta)\,\vec{n}
\end{aligned} \tag{B.6}$$

in the c.m. system.

ACKNOWLEDGEMENTS

I would like to thank a number of people without whom the completion of this report would have been impossible.

First of all I wish to express my appreciation to Professors K. Miyake and T. Nakamura for their continuous encouragements and guidances throughout the course of this experiment. Their suggestions during the course of this analysis were invaluable.

I am also grateful to Drs. R. Kikuchi, Y. Hemmi, T. Miyachi, N. Tamura, K. Imai, M. Yoshioka and I. Nakao and Messrs. A. Ando, H. Sato, A. Noda and M. Ono for their advices and collaboration in carrying out this experiment.

The late Dr. N. Yamashita was my good partner. His work on every stage of this experiment were greatly appreciated.

In addition I would like to thank the technical staff and the operation crew of the INS electron synchrotron for their excellent operation.

Finally I would like to thank the members of the machine shop under Mr. S. Hanazono in constructing the π° detection system.

The numerical calculation were performed by the TOSBAC-3400 at the INS and the FACOM230/75 at the Computor Center of Kyoto University.

REFERENCES

1) D. Faiman and A. W. Hendry, Phys, Rev. **180** (1969) 1572.
2) L. A. Copley, G. Karl and E. Obryk, Phys. Letters **29B** (1969) 117.
3) R. P. Feynman, Kislinger and F. Ravndal, Phys. Rev. **D3** (1971) 1706.
4) H. Sugimoto and M. Toya, Prog. Theor. Phys. **55** (1976) 1488.
5) J. T. Beale, S. D. Eklund and R. L. Walker, California Inst. of Technology Report CTSL-42 CALT-68-108 (1966).
6) P. Spillantini and V. Valente, CERN-HERA 70-1 (1970).
7) H. Genzel and W. Pfeil, Bonn Univ. Report PI Bl-168 (1972).
8) Y. Inagaki, T. Nakamura and K. Ukai, INS Report INS-TH-109 (1976); T. Nakamura and K. Ukai, INS Report INS-TH-116 (1977).
9) Y. Hemmi, T. Nakamura, R. Kikuchi, A. Maki, K. Miyake, T. Inagaki, A. Sasaki, N. Tamura, S. Yasumi and H. Okuno, Nucl. Phys. **33** (1974) 333; Phys. Letters **32B** (1970) 137.
10) C. Bacci, R. Baldini-Celio, B. Esposito, C. Menuccini, A. Reale, G. Sciacca, M. Spinetti and A. Zallo, Phys. Letters **39B** (1972) 559; Lett. Nuovo Cimento **4** (1972) 5.
11) R. W. Clifft, E. Gabathuler, L. S. Littenberg, R. Marshall, S. E. Rock, J. C. Thompson, D. L. Ward and G. R. Brooks, Phys. Rev. Letters **33** (1974) 1500.
12) E. Di Capua, V. Pocci, M. Severi, L. Tau, E. Fiorentino, F. Palmonari, A. Reale, L. Satta and G. Ubaldini, Lett. Nuovo Cimento **8** (1973) 692.
13) D. I. Julius, For. der Physik **22** (1974) 311.
14) A. I. Sanada and G. Shaw, Phys. Rev. **D3** (1971) 243; Phys. Rev. Letters **24** (1970) 1310.
15) A. I. Sanada and G. Shaw, Phys. Rev. Letters **26** (1971) 1057; A. Donnachie, Proc. 5th Int. Symp. on Electron and Photon Interactions at High Energies, Ithaca, New York, 1971.
16) G. Von Holtey, G. Knop, H. Stein, J. Stümtig and H. Wahlen, Phys. Letters **40B** (1972) 589.
17) T. Fujii, S. Homma, K. Huke, S. Kato, H. Okuno, F. Takasaki, T. Kondo, S. Yamada, I. Endo and H. Fujii, Phys. Rev. Letters **28** (1972) 1672.
18) N. Yamashita, Memoirs of the Faculty of Science, Kyoto Univ. **35** (1977) 35.
19) K. Ukai, private communication.
20) I. Nakano, private communication.
21) A. Sørenssen, Nuovo Cimento **38** (1965) 745.
22) T. Miyachi et al., J. Phys. Soc. Japan **33** (1972) 577.
23) H. E. Jackson et al., Phys. Rev. **119** (1960) 1381; J. I. Vette et al., Phys. Rev. **111** (1958) 622, D. B. Miller et al., Proc. Phys. Soc. of London **81** (1963) 343; W. Hitzeroth et al., Nuovo Cimento **60** (1969) 467; R. Diebold et al., Phys. Rev. **130** (1963) 2089; J. S. Barton et al., Nucl. Phys. **B84** (1975) 449; P. S. L. Booth et al., Duresbury Report DNPL-P95 (1971); Y. Hemmi et al., Nucl. Phys. **B55** (1972) 333; G. Fisher et al., Zeit. für Physik **245** (1971) 225; C. Bacci et al., Phys. Rev. **159** (1967) 1124; J. W. Dewire et al., Phys. Rev. **110** (1958) 1208; F. Wol-

verton, Ph. D thesis (1968); R. L. Walker et al., Phys. Rev. **97** (1954) 1279; R. Morand et al., Phys. Rev. **180** (1969) 1229; W. Brauschweig et al., Zeit. für Physik **245** (1971) 253; D. C. Oakley et al., Phys. Rev. **97** (1955) 1283; P. Dougan et al., Zeit für Physik **A274** 73; P. C. Stein et al., Phys. Rev. **110** (1958) 1209; H. Genzer et al., Born Report PI BI–152 (1972); S. Almehed et al., Bonn Conf. (1973); C. Ward et al., Phys. Rev. **159** (1967) 1176; D. E. Lundquist, Ph. D. thesis (1967); H. De. Staebler et al., Phys. Rev. **140** (1965) B336; R. L. Walker et al., Phys. Rev. **89** (1953) 1301.

24) R. G. Moorhouse, H. Oberlack and A. H. Rosenfeld, Phys. Rev. **D9** (1974) 1.
25) W. J. Metcalf and R. L. Walker, Nucl. Phys. **B76** (1974) 253.
26) E. Gabathuler and G. Shaw, Daresbury Report DL/32 (1973).
27) R. J. Glauber, Phys. Rev. **100** (1955) 242.
28) V. Franco and R. J. Glauber, Phys. Rev. **142** (1966) 1195, ibid. **156** (1967) 1685.
29) M. Goldberger and K. Watson, Collision Theory (John Wiley & Sons, Inc., New York, 1964).
30) G. Fäld, Nucl. Phys. **B29** (1971) 16.
31) G. C. Fox and C. Quig, Compilation of elastic scattering data, UCRL–20030 πN (1970).
32) R. Baldini-Calio and G. Sciacca, Frascati Report LNF–71/92 (1971).
33) T. Fujii, T. Kondo, F. Takasaki, S. Yamada, S. Homma, K. Huke, S. Kato, H. Okuno, I. Endo and H. Fujii, Nucl. Phys. **B120** (1977) 395.
34) C. F. Chew and H. W. Lewis, Phys. Rev. **84** (1951) 779.
35) P. Bentz et al., Nucl. Phys. **B65** (1973) 158.
36) I. G. Aznauryan, Sov. J. Nucl. Phys. **19** (1974) 324.
37) Y. Yoshimura, S. Hatano, Y. Hemmi, R. Kikuchi, S. Kobayashi, K. Miyake, T. Nakamura, H. Okuno and S. Yasumi, J. Phys. Soc. Japan **24** (1968) 1395.